Thermo-mechanical FE-analysis
butt-welding of a Cu-Fe canister
spent nuclear fuel

B L Josefson[1], L Karlsson[2], L-E Lindgren[2], M Jon

1 Chalmers University of Technology, Göteborg, S
2 Division of Computer Aided Design, Luleå
University of Technology, Luleå, Sweden

October 1992

SKB-TR--9

THERMO-MECHANICAL FE-ANALYSIS OF BUTT-WELDING OF A CU-FE CANISTER FOR SPENT NUCLEAR FUEL

B L Josefson[1], L Karlsson[2], L-E Lindgren[2], M Jonsson[2]

1 Chalmers University of Technology, Göteborg, Sweden
2 Division of Computer Aided Design, Luleå University of Technology, Luleå, Sweden

October 1992

This report concerns a study which was conducted for SKB. The conclusions and viewpoints presented in the report are those of the author(s) and do not necessarily coincide with those of the client.

Information on SKB technical reports from 1977-1978 (TR 121), 1979 (TR 79-28), 1980 (TR 80-26), 1981 (TR 81-17), 1982 (TR 82-28), 1983 (TR 83-77), 1984 (TR 85-01), 1985 (TR 85-20), 1986 (TR 86-31), 1987 (TR 87-33), 1988 (TR 88-32), 1989 (TR 89-40), 1990 (TR 90-46) and 1991 (TR 91-64) is available through SKB.

Keywords: electron beam welding, residual stresses, canister, copper, finite element.

THERMO-MECHANICAL FE-ANALYSIS OF BUTT-WELDING OF Cu-Fe CANISTER FOR SPENT NUCLEAR FUEL

B. L. Josefson, Division of Solid Mechanics, Chalmers University of Technology, S-412 96 Göteborg, Sweden

L. Karlsson, L.-E. Lindgren and M. Jonsson, Division of Computer Aided Design Luleå University of Technology, S-951 87 Luleå, Sweden

ABSTRACT
(English)

In the Swedish nuclear waste program it has been proposed that spent nuclear fuel shall be placed in composite copper - steel canisters. These canisters will be placed in holes in tunnels located some 500 m underground in a rock storage. The canister consists of two cylinders of 4850 mm length, one inner cylinder made of steel and one outer cylinder made of copper. The outer diameter of the canister is 880 mm and the wall thickness for each cylinder is 50 mm. At the storage, the steel cylinder, which contains the spent nuclear fuel, is placed inside the copper cylinder. Thereafter, a copper end is butt welded to the copper cylinder using electron beam welding. To obtain penetration through the thickness with this weld method a backing ring is placed at the inside of the copper cylinder.

In the present work, the temperature, strain and stress fields present during welding and after cooling for welding are calculated numerically using the FE-code NIKE-2D. The aim is to use the results of the present calculations to estimate the risk for creep fracture during the subsequent design life. A large strain formulation is employed for the calculation of transient and residual stresses in the canister based on the calculated history of the temperature field present in the canister during the welding process. The contact algorithm available in NIKE-2D is used to detect possible contact between the steel and copper cylinders during the welding. To simplify the numerical calculations and reduce the computational time, rotational symmetry is assumed.

For large gap distances between the steel and copper cylinders the residual stress field is calculated to have a shape similar to that observed in butt welded pipes with maximum axial stress values at the yield stress level. For small gap distances the backing ring will come in contact with the steel cylinder which leads to large residual stresses in the backing ring. The maximum accumulated plastic strain in the weld metal and HAZ was calculated to about 5 % for both gap distances.

(Swedish)

I det svenska kärnavfallsprogrammet har det föreslagits att det använda kärnbränslet skall placeras i en koppar - stål kompositkapsel. Dessa kapslar kommer att placeras i hål i tunnlar cirka 500 m under markytan i ett bergförvar. Kapseln består av två cylindrar med 4850 mm längd; en inre cylinder gjord av stål och en yttre cylinder gjord av koppar. Kapselns yttre diameter är 880 mm och väggtjockleken för vardera cylindern är 50 mm. Vid förvaret placeras stålcylindern, som innehåller det använda kärnbränslet, inuti kopparcylindern. Därefter stumsvetsas ett kopparlock fast på kopparcylindern med elektronstrålesvetsning. För att kunna få penetration genom hela godset med denna svetsmetod har ett rotstöd i form av en kopparring placerats inuti kopparcylindern.

I rapporten beräknas temperatur, töjnings och spänningsfälten under svetsning och efter kylning efter svetsning numeriskt med hjälp av FE-koden NIKE-2D. Syftet är att använda resultaten från beräkningarna till att bedöma risken för krypbrott under den period kapseln konstruerats för att hålla. Stora töjningars teori används för beräkningen av transienta och kvarstående spänningar i kapseln baserat på den beräknade temperaturfördelningen i kapseln under svetsförloppet. Kontaktalgoritmen i NIKE-2D används för att spåra eventuell kontakt mellan stål och kopparcylindrarna under svetsningen. För att förenkla de numeriska beräkningarna och för att minska beräkningstiden antas rotationssymmetri.

Då det finns ett stort gap mellan stål och kopparcylindrarna beräknas restspänningsfältet vara liknande det som observeras i stumsvetsade rör med maximal axialspänning i nivå med sträckgränsen. För fallet små gap kommer rotstödet i kontakt med stålcylindern, vilket leder till stora restspänningar i rotstödet. Den maximala plastiska töjningen i svetsgodset och i den värmepåverkade zonen beräknades till cirka 5 % för båda fallen.

Thermo-mechanical FE-analysis of butt-welding of a Cu-Fe canister for spent nuclear fuel

B L Josefson, Division of Solid Mechanics, Chalmers University of Technology, S-412 96 Göteborg, Sweden

L Karlsson, L-E Lindgren and M Jonsson, Divison of Computer Aided Design, Luleå University of Technology, S-951 87 Luleå, Sweden

INTRODUCTION

The highly radioactive spent nuclear fuel produced in Swedish power reactors shall be placed in an underground storage after intermediate storage in water basins for forty years. The primary altenative design for this final storage is to place canisters containing the waste in vertical holes in the floor of horizontal tunnels located in granite rock several hundred meters below earth's surface. Each cylinder will be surrounded by a 40 cm thick clay barrier which is supposed to reduce the outward flow of radioactive particles from a possibly leaking corroded canister.

The canister consists of two concentric cylinders, an inner steel cylinder containing the spent nuclear fuel, and an outer copper cylinder. When the canister is loaded with waste the steel cylinder is placed inside the copper cylinder. Thereafter, the canister is sealed by butt-welding a copper end to the copper cylinder by use of Electron Beam Welding (EBW). This method produces a very narrow weld zone without the use of a filler metal, and it can penetrate into large depths in one weld pass. To ensure full penetration of a weld through the thickness of the copper cylinder a backing ring made of copper is placed inside the copper cylinder. Half the distance of this backing ring is penetrated by the electron beam.

Present investigation The canister will be loaded by the residual stresses caused by the welding process, by an outer pressure from the clay (and surrounding rock mass), and by possible tectonic movements in the rock mass. The ultimate goal of the mechanical investigations initiated by the Swedish Nuclear Fuel and Waste Management (SKB) is to investigate the long term mechanical stability of the canister as subject to these loads. However, this paper focusses on the residual stresses and plastic strains caused by the sealing butt-welding of the copper cylinder. At this point, one may note, that although this is the primary alternative canister design (there are alternative designs both for the storage outline and the canister design) details of the canister geometry, canister loading procedure, and the electron beam welding process are still uncertain. Only one parameter will be varied in the present paper, the gap (clearance) between the steel cylinder and the copper cylinder. A large gap distance is desired to simplify the loading of the 5 m long heavy steel cylinder into the copper cylinder. However, it is easy to realize that this distance may be vey small at some places, which will affect the thermal flow in the canister. One pilot butt-welding of a copper cylinder by use of electron beam welding was made at the Welding Institute

(TWI), see [1]. The aim with that investigation was to see if electron beam welding was a feasible welding process. Low residual strains were measured in the copper cylinder after the welding.

Although there exist formulas and simplified methods for estimations of axial stresses in butt-welded pipes, see for example [2-4], it is difficult to predict, beforehand, the residual stress level in the butt-welded canister. Firstly, the weld is located close to the plane end that, together with the presence of a thick backing ring, increases the stiffness of the part of the canister located above the butt weld. Hence, the geometry differs considerably from the butt-welded pipe case. Secondly, the electron beam weld process uses a very high heat input. It is hard to use formulas from [2] even if they are based on the ratio of heat input over wall thickness. In the present case both factors have values outside the span used when finding constants for the empirical formulas in [2]. Therefore, we propose that the residual stresses are calculated numerically by first simulating the temperature field present in the canister and thereafter calculating the corresponding mechanical strain and stress fields. Similar FE-analyses have been performed before by the present authors see for example [5-7].

The transient and residual temperature field and stress and strain fields present in the canister during welding and after cooling to ambient temperature is calculated numerically by use of the commercial FE-codes TOPAZ2D [8] and NIKE2D [9].

The canister has the total length 4850 mm and the outer diameter 880 mm. The wall thickness of each of the two cylinders is 50 mm. The thickness of the backing ring is also 50 mm. The steel material is an ordinary C-Mn steel and the copper material is an OFHC alloy with the room temperature yield stress 50 MPa. The plane copper end is butt welded to the copper cylinder in one weld pass by use of electron beam welding. Figure 1 shows the geometry of the canister and a blow-up of the weld geometry.

As indicated above only one geometrical parameter will be varied in the present study, namely the gap distance between the steel and copper cylinder. The gaps studied here are 0.2 mm and 2.0 mm. Note that these gaps are measured for a heated inner cylinder, hence the gap distances will change when the copper cylinder is heated and thereafter cooled during the welding.

FE-MODEL

For thin-walled pipes, it is often found that the welding residual deflections and axial stresses in a butt-welded pipe are similar in shape to that of a pipe subject to a circumferential line load. Thus, the residual deflection is localized to the weld region (or the location of the line load). Standard text books in Strength of materials will give an estimate of the axial extent of the region with prevailing bending deflections. For the present dimensions of the canister, Fig. 1, it is found that it is sufficient to study 1 m of the canister in the axial direction. A cross sectional area of this part of the canister is divided into 1250 bilinear 4-node elements assuming rotational symmetry, see Fig. 2. This FE-mesh

consists of 1341 nodes. Although the transient stress field present in a welded pipe is strongly non-rotationally symmetric, the residual stress is often found to be reasonably rotationally symmetric, in particular when the welding speed used was high, see for example [10]. With a high welding speed the heat conduction close to the heat source will be primarily oriented transverse to the heat source, that is in the axial direction of the pipe. However, the main reasons for adopting a rotationally symmetric FE-model in the present study are to reduce (considerably) the size of the model and to limit the CPU-time needed. Physically, the welding speed is normally high in electron beam welding, but the high thermal conductivity in copper will lead to a high heat flux also in the direction parallel to the heat source. This will reduce the validity of the assumption of rotational symmetry. The same FE-mesh has been used for both the thermal and mechanical analyses. Formally, this means that the mechanical strain field and thermal strain field will be incompatible. Therefore, in each element the temperature is taken as constant, that is the average temperature value from the four corner nodes is assigned to the center of the element, within each element to give the same spatial variation for the mechanical and thermal strains. To model contact conditions slidelines have been applied between the inner steel cylinder and the outer copper cylinder and between the inner steel end and the outer copper end.

FE-CALCULATIONS

Preliminaries The thermal and mechanical field are formally coupled through the presence of a thermal strain in the mechanical analysis, and a strain rate term in the thermal analysis (heat conduction equation). However, for welding problems it has been found that this latter term can be neglected, see for example [11], which means that the heat generated by deformations is not considered. Hence, the analysis can be divided into two parts. First the temperature field due to the heat input is calculated and secondly the mechanical analysis is performed with the previuosly calculated history of the temperature field as load. Note, that both the thermal and the mechanical analyses are strongly nonlinear due to the temperature dependence of the material properties and the possible contact between the steel and copper cylinders.

This contact between the inner steel and outer copper cylinder will also, formally, couple the thermal and mechanical analysis. The gap between the cylinders, which may be zero at some points, is calculated in the mechanical analysis. However, it also enters in the thermal analysis as a part of the contact resistance between the two cylinders, see for example [12]. Since the version of NIKE2D used does not have the option of performing a fully coupled thermal and mechanical analysis, it was decided to account for this coupling approximately. Thus, the contact resistance in the thermal analysis was taken as constant in time and the zones in contact were estimated from initial mechanical calculations.

Thermal analysis The FE-code TOPAZ2D [8] has been used to calculate the transient temperature fields in the canister due to welding. The inner steel cylinder was assumed to have a constant temperature of 180°C and the outer copper cylinder and the copper end were at room temperature, 20°C, when the heat input was applied. In the calculations the

heat was applied for three seconds with a net heat input of 24 MJ/m and a corresponding welding speed of 100 mm/min. These values are believed to be a suitable combination that would give a good EBW for 50 mm thick copper material [13].

The heat was introduced in a volume (width = 4 mm and inner and outer radius = 365 and 440 mm respectively) at the interface between the copper end and the upper end of the copper cylinder, see Fig. 1. Thus the weld is assumed to penetrate half the thickness of the backing ring. The strength of the heat input was constant across the thickness of the cylinder and backing ring. The three seconds of heat input were divided into 275 time increments and the subsequent cooling to room temperature (reached at t = 2400 s) with 110 time increments. For each time increment the temperature field was stored for use as input in the subsequent mechanical analysis.

Thermal material data The temperature variation of thermal properties for the ordinary steel used is well known. It is more difficult to obtain the corresponding values for the copper alloy used in the outer cylinder. Here we have used values supplied by the manufacturer, [14] and from handbooks in Physics. Figures 3a and 3b show the temperature variation of the thermal conductivity and heat capacity used. The value of latent heat for the solid to fluid phase transformation in copper used is 205 kJ/kg, and the liquidus temperature is 1083 °C. The free convective surface heat transfer coefficient for the copper cylinder and end is taken from [15], see Fig. 4. The temperature variation for this heat transfer coefficient also accounts for radiative surface heat transfer. The inner surface of the steel cylinder was assumed to have a constant temperature (180 °C) boundary condition during the entire time history. The boundary condition at the lower end of the FE-model (z = 0.930 m) is taken the same as for the outer surfaces of the cylinders. The boundary at r = 0, that is the axis of symmetry, for the two end is taken as isolated. The convection and radiation between the outer surface of the steel cylinder and the inner surface of the copper cylinder is modelled with a thermal contact resistance according to Madhusudana and Fletcher [16] and Kristiansson [12]. Hence, the heat transmission coefficient h is

$$\frac{1}{h}=\frac{1}{h_0}+\frac{d}{k_g} \tag{1}$$

Here $1/h_0$ is a small contact resistance representing non-perfect contact, k_g the thermal conductivity of the gas in the gap and d is the gap. The values chosen in the analyses were k_g= 0.10 W/m°C and h_0= 1000 W/m²°C. Perfect contact was assumed between the copper cylinder and the upper and right boundary surfaces of the backing ring. This means that the two cases differ only in gap distance and resulting different values for the thermal contact resistance.

Mechanical analysis The mechanical analysis was performed for t = 0 s to t = 1700 s, using 120 time increments for the welding process and 150 time increments for the cooling process. We have have found that use of these time steps gave results that were insensitive to the time step length. Use of much larger time steps may give results that converge (nodal force equilibrium is achieved) but the accumulation of plastic strain may not be accurately

followed. The transient temperature fields calculated in the thermal analysis have been used as thermal load in each time step in the mechanical analyses. No mechanical load is applied to the canister in this analysis. Hence the pressure load from the surrounding clay barrier, or prescribed displacements caused by tectonic movements are not considered here. The FE-code NIKE2D [9] was used in the mechanical calculations. The theory for large strains available in NIKE2D is employed, hence the resulting non-linear FE-equations to be solved are:

$$[K]^{(i-1)}_{t+\Delta t}\{\Delta U\}^{(i)}_{t+\Delta t} = \{R\}_{t+\Delta t} - \{F\}^{(i-1)}_{t+\Delta t} \tag{2}$$

The system of Equations (2) are solved iteratively using the BFGS-method including line-searches to obtain the displacement vector $\{U\}_{t+\Delta t}$ at the end of each load step. To achieve equilibrium the error in Euclidian norm of displacement increments and in the energy norm (calculated as the product of displacement increment and nodal force residual) shall be less than 0.1 % and 1 % respectively. About 2 - 4 iterations were needed to establish equilibrium in each load step.

In Eqn (2), the stiffness matrix [K] is the sum of the ordinary linear stiffness matrix and the geometric stiffness matrix. The vector { F } is a vector of "internal" nodal forces that are equivalent to Cauchy stresses within each element. With elements of the Cauchy stress tensor τ_{kl} in each point collected in a stress vector { τ } one obtains

$$\{F\}^{(i-1)}_{t+\Delta t} = \sum_{m=1}^{numel} \int_{V_m} [B]^T \{\tau\}^{(i-1)}_{t+\Delta t} dV_m \tag{3}$$

This vector is evaluated at the end of each load step. Here [B] is the nonlinear strain matrix and i denotes the iteration count for the global equilibrium iterations. The integrals in Eqns (2,3) are evaluated using Gaussian quadrature and 1x1 integration points per element. The increase in Cauchy stress in a Gaussian point during one iteration is evaluated by use of the Green-Naghdi stress rate and the increase in strain $\Delta\varepsilon$ calculated from $\{\Delta U\}_{t+1/2\Delta t}$ at the mid-point of the time step, see [9] for details. The gap between steel and copper cylinders is modelled with slidelines, which means that if contact is detected in certain points global iterations are performed to find the displacement fields using a penalty approach. Since there is no mechanical load applied the external load vector { R } will only contain surface pressures due to possible contact between the cylinders. The boundary conditions used in the mechanical analyses are shown in Fig. 2.

Mechanical material data In the calculations the copper material is assumed to be thermo-elasto plastic. The temperature dependent material properties used for copper; yield stress, Youngs modulus, Poissons ratio, thermal strain and hardening modulus are shown in Figs. 5-9. The temperature dependence of Poisson's ratio was found in [17] and the other material properties were obtained from the copper manufacturer [14]. Isotropic hardening

and an associated flow rule is adopted. The values for the hardening modulus are estimated from stress - strain curves from [14] assuming a linear $\sigma - \varepsilon^p$ variation of the hardening modulus up to plastic strains of 15 %. The steel was assumed to be thermo-elastic. The temperature dependent material properties for steel; Youngs modulus, Poisson's ratio and thermal strain were taken from [7]. The thermal strain is defined as the linear thermal expansion coefficient integrated from the reference temperature to the actual temperature.

Parts of the material located in the HAZ will accumulate compressive plastic strains as it is rapidly heated when the heat source is applied. For gaussian points in this region that melts, plastic strains accumulated before (and during) melting are defined as inelastic strains and they are not used for the calculation of hardening during the subsequent cooling phase. With this approach, hardening in one phase does not depend on plastic deformation experienced in a previous phase.

CALCULATED RESULTS

Thermal results The gap distance will have a small influence on the temperature field during the early stages of cooling. Figure 10 shows calculated isoterms in the weld region when the maximum temperature is roughly 1400 °C. It is clearly seen that the gap isolates the steel cylinder from the copper cylinder even if there will be contact at the backing ring for small gap distances. During this initial part of the cooling the width of the gap does not influence the temperature field. This is due to the very narrow weld zone, see Fig. 10. The corresponding highest temperature calculated for the steel canister was 240 °C.

Figure 11 shows the calculated temperature history for one point located in the weld zone. The plateaus in the temperature curve are due to the phase changes from solid to fluid phases. With the proposed prescribed heat input the material will be heated way above the melting temperature. Although very difficult to verify experimentally, there are indications in the literature that, during welding, material that melts will be heated several hundred degrees (°C) above the melting temperature. The remote part of the pipe located 1 m from the end (in the axial direction) was found to have a uniform temperature field (and resulting membrane stress state) during the analysis. This justifies the axial extent of the cylindrical part of the canister.

Mechanical results During the welding material located close to the weld line will be subject to a strong temperature increase and corresponding development of thermal strain. Since the surrounding material is much cooler (and thus stiffer) strong compressive stresses will develop in the weld zone. The magnitude of these stresses is controlled by the yield stress value at the actual temperature. When the welding is completed this part of the canister cools rapidly and wants to contract, at the same time the temperature in the surrounding material is slowly increasing. ***For a large gap, that is 2.0 mm,*** there will be no contact between the copper and steel cylinders (except initially in some few points). Thus, the stresses in the weld metal will then increase and become tensile. Figures 12 a-b show calculated axial and hoop stresses at a point located some 10 mm below the weld line and

some 30 mm from the inner surface of the copper cylinder, point A in Fig. 2. For large gaps the copper cylinder will act as a butt welded pipe. The stiff copper end will restrict the cross sectional rotation of the copper canister at the lower surface of the backing ring. This creates a bending moment that is the resultant of tensile axial stresses at the inner surface of the copper canister and compressive axial stresses at the outer surface. Figures 13 a-b show isolines for the welding residual axial and hoop stresses in the copper cylinder. The axial stress distribution typical for a butt welded pipe (where a large heat input over wall thickness has been employed) is clearly displayed. It is more difficult to predict the shape and magnitude of the residual hoop stress. However, as seen in Fig. 13b, the stress concentration at the lower right corner of the backing ring seems to increase the hoop stresses as compared to the butt welded pipe case. During the welding the radial stresses in the weld region have values similar to those in Figs. 12 a and b thus indicating a nearly hydrostatic stress state in this region. During the cooling when the heat is conducted the stress state becomes somewhat more bi-axial except at the stress concentration discussed above. The maximum residual von Mises effective stress is calculated for the stress concentration point. The value, roughly 120 MPa, indicate a strong hardening in this point.

For ***the small gap, 0.2 mm***, initial calculations revealed that the inner vertical surface of the backing ring will come in contact with the steel cylinder. This surface remained in contact during the cooling phase. Contact was also detected at some points of the lower horizontal surface of the backing ring. To simulate the influence of the contact at the inner surface of the backing ring, the thermal analysis for the small gap case was rerun with the distance d = 0 in Eqn (1) for this surface of the backing ring (and using d = 0.2 mm) for other potential contact surfaces. Figures 14 a,b show calculated transient axial and hoop stresses for point A (see Fig. 2). It is seen that the contact results in compressive axial and hoop stresses during cooling instead of tensile as in Figs. 12 a,b. Isolines for the welding residual axial and hoop stresses for this gap are shown in Figs. 15 a,b. For this case the axial stresses are controlled by the contact giving large tensile values near the inner surface of the backing ring that are balanced by low stresses in the weld region.

The residual stresses in the steel cylinder were found to have roughly the same maximum values as in the copper canister. For the small gap case, the largest effective stress was 150 MPa just below the lower left corner of the backing ring. Large hoop stresses, 160 MPa, were also calculated just below the copper end. However, with the higher value for the yield stress in the steel used, σ_Y = 300 MPa, the assumption of elastic conditions in the steel cylinder seems to be justified.

An entity of special interest in the copper cylinder is the accumulated plastic strain. High values for this entity would indicate an increased risk for creep fracture. Isolines for the calculated residual effective plastic strains for the two gap distances are shown in Figs. 16 and 17. One finds that plastic strains are concentrated to the stress concentration at the lower right corner of the backing ring and to the HAZ close to the weld. Note that the displayed plastic strains do not include plastic strains accumulated prior to and during melting. Hence plastic strains in the weld zone are lower than in the HAZ just outside the

weld zone. The maximum values are calculated in the backing ring for both gaps and they are 13% and 5% for 2.0 mm and 0.2 mm gap respectively. In the HAZ the maximum value was found to be 5 % for both gaps. Considering the rough geometrical modelling of the stress concentration one may conclude that the accumulated plastic strains seem to acceptably low.

Figure 18 shows the accumulation effective plastic strain during the cooling phase for a point in the backing ring in its lower right corner for the large gap case. The corresponding temperature history for this point is shown in Fig. 19. One finds that the major part of the plastic strain is accumululated during and immediately after the welding. However, material in this point, which is highly loaded, seems to yield continuously during the entire cooling phase.

DISCUSSION

As discussed above, to obtain FE-calculated results using a reasonable amount of CPU-time some simplifications have to be made in the present model. The most important simplification is of course the assumption of rotational symmetry. Even if it is hard to justify this assumption from physical reasons (due to the high conductivity for copper), we believe that our results will give a good estimate of the residual stress state. Our experience is that, see [5,6,10], the residual stress state after circumferential butt welding tend to be reasonably rotationally symmetric.

One may also emphasize that we still have insufficient knowledge of elasto-plastic behaviour of copper during rapid cooling from elevated temperatures. Moreover, the welding parameters used in the present calculations were supplied to us as estimates based on a limited number of EBW experiments on 100 mm thick copper.

Our conclusion is that the welding residual stresses and residual plastic strains seem to be acceptably low in the copper cylinder for reasonable values of the gap between the two cylinders. Large stresses are calculated for the lower right corner of the backing ring that were not modelled in detail here.

For future work we suggest that it is important to design (and FE-model) the backing ring more accurately. It is also essential to investigate the procedure for loading of the steel cylinder (containing the spent fuel) into the copper cylinder in detail. To ensure a safe loading, the gap between the two cylinders will probably have to be larger than the 2.0 mm used here. A temperature difference of 200 °C between the steel and copper cylinders will, for example, correspond to a reduction of the gap distance with roughly 0.5 mm.

REFERENCES

1 R.H. Leggatt, Residual stress measurements in a EB welded copper disc, SKB/KBS Technical Report TR 83-25, Swedish Nuclear Fuel and Waste Management Co, Stockholm, Sweden, (1983).

2 A. Scaramangas and R.F.D. Porter Goff, Residual stresses in cylinder girth butt welds, 17th annual Offshore Technology Conference, Houston, TX, (1985), Paper 5024.

3 R.H. Leggatt, Residual stresses at circumferential welds in pipes, *Welding Institute Research Bulletin*, 23 (1982) 181-188.

4 B.L. Josefson, Prediction of residual stresses and distortions in welded structures, *Proceedings of The 10th International Conference on Offshore Mechanics and Arctic Engineering, Vol III, Part A*, ed. M.M. Salama, M. Toyoda, S. Liu, J.F. Dos Santos and M.Kocak (ASME, New York, 1991) pp. 25-30. Accepted for publication in *ASME Journal of Offshore Mechanics and Arctic Engineering*.

5 B.L. Josefson, M. Jonson, L. Karlsson, R.I. Karlsson, C.T. Karlsson and L.-E. Lindgren, Transient and residual stresses in a single-pass butt welded pipe, in: *International Conference on Residual Stresses ICRS2*, ed. G. Beck, S. Denis and A. Simon (Elsevier Applied Science, London, 1989) pp. 497-503.

6 R.I. Karlsson and B.L. Josefson, Three-dimensional finite element analysis of temperatures and stresses in a single-pass butt-welded pipe, *ASME Journal of Pressure Vessel Technology*, 112 (1990) 76-84.

7 M. Jonsson, L. Karlsson and L.-E. Lindgren, Deformations and stresses in butt-welding of large plates, in: *Numerical Methods in Heat Transfer, Vol III*, ed. R. W. Lewis (John Wiley & Sons, Chichester, UK, 1985), pp. 35-58.

8 A.B. Shapiro, TOPAZ2D-A two dimensional finite element code for heat transfer analysis, electrostatic, and magnetostatic problems, report UCID-20824, Lawrence Livermore National Laboratory, Berkeley, CA (1986).

9 B.E. Engelmann, NIKE-2D A nonlinear,implicit, two-dimensional finite element code for solid mechanics - User's manual, Report UCRL-MA-105413, Lawrence Livermore National Laboratory, Berkely, CA (1991)

10 M. Jonsson and B.L. Josefson, Experimentally determined transient and residual stresses in a butt-welded pipe, *Journal of Strain Analysis*, 23, (1988) 25-31.

11 J.H. Argyris, J. Szimmat and K.J. Willam, Computational aspects of welding stress analysis, *Computer Methods in Applied Mechanics and Engineering*, 33 (1982) 635-666.

12 J.-O. Kristiansson, Thermomechanical behaviour of the solidifying shell within continuous-casting billet molds - a numerical approach, *Journal of Thermal Stresses*, 7 (1984) 209-226.

13 A. Sanderson, The Welding Institute, Abington, UK (1992) Private communication.

14 H. Rajainmäki, Outokumpu Pori Copper OY, Pori, Finland (1992) Private communication.

15 J.H. Argyris, J. Szimmat and K.J. Willam, Finite element analysis of arc-welding processes, Proceedings of The Third International Conference on Numerical Methods in Thermal Problems, Pineridge Press , Swansea, UK, (1983) pp. 249-258.

16 C.V. Madhusudana and L.S. Fletcher, Contact heat transfer - the last decade, *AIAA Journal*, 24 (1985) 510-523.

17 J.F. Bell, The experimental foundations of solid mechanics, *Mechanics of Solids, Vol I* (Springer Verlag, Berlin, Germany, 1984) pp. 280.

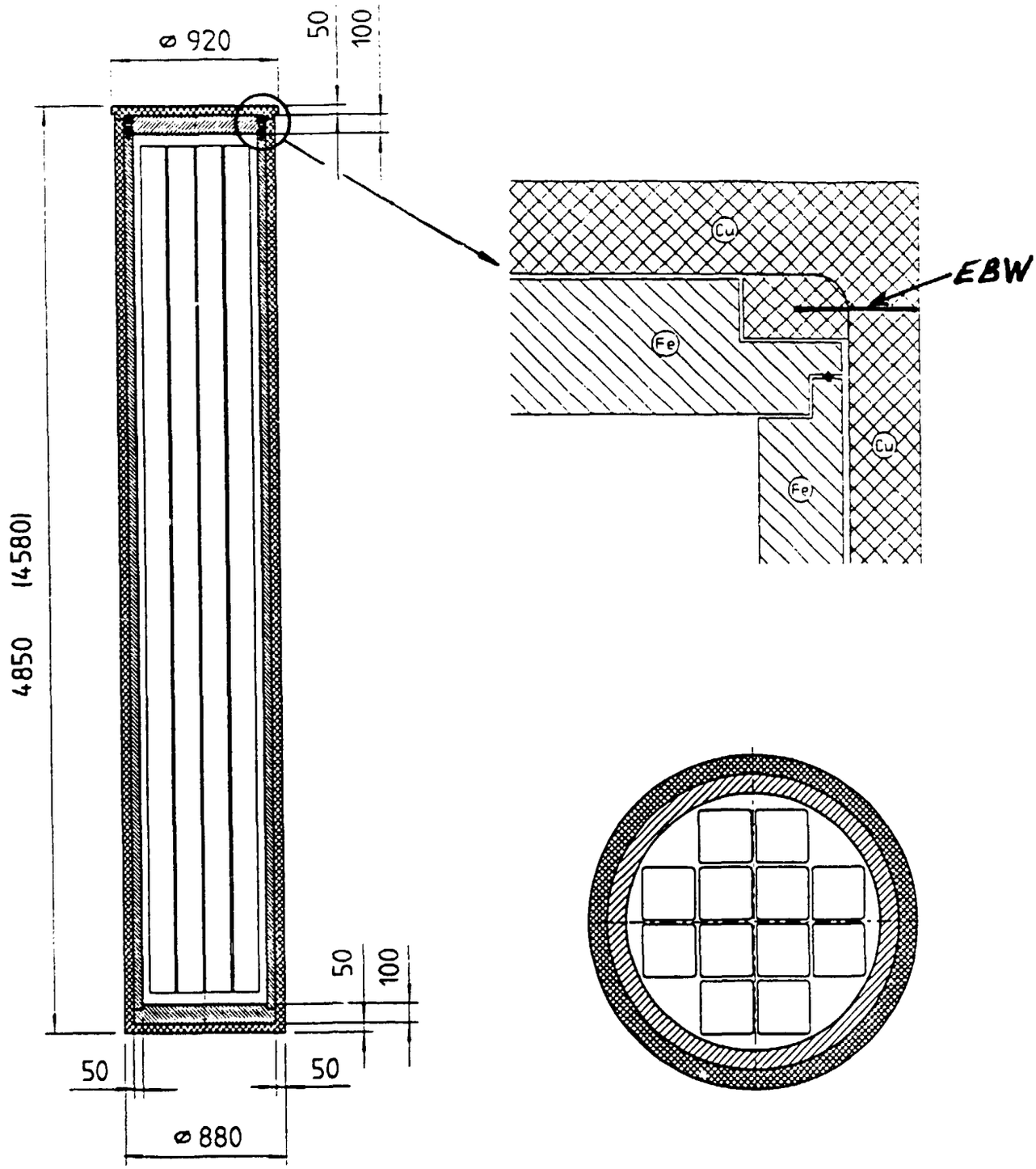

Fig 1 Geometry of the canister

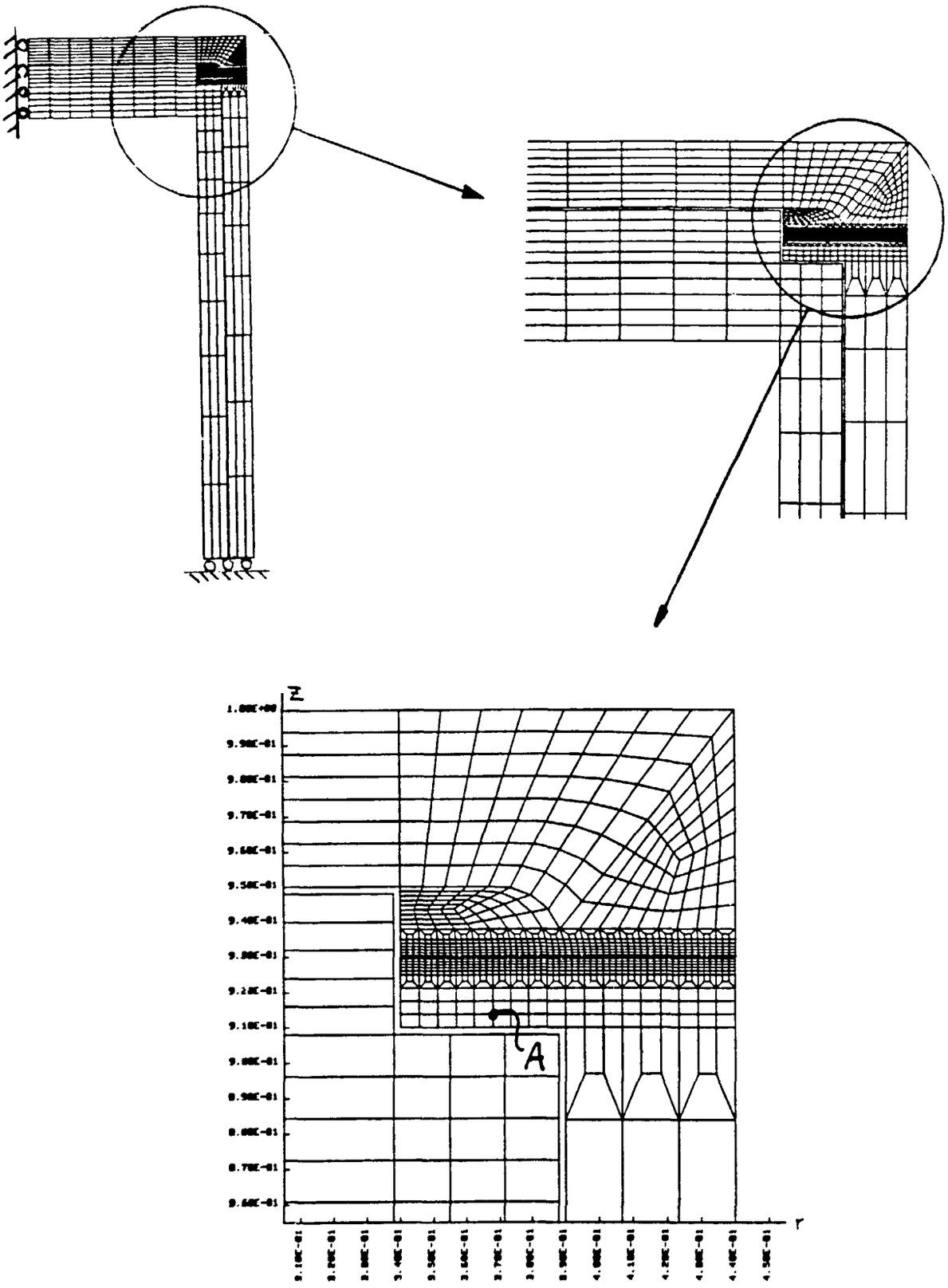

Fig 2 Finite element mesh used in both thermal and mechanical analyses. Point A is used for result presentations.

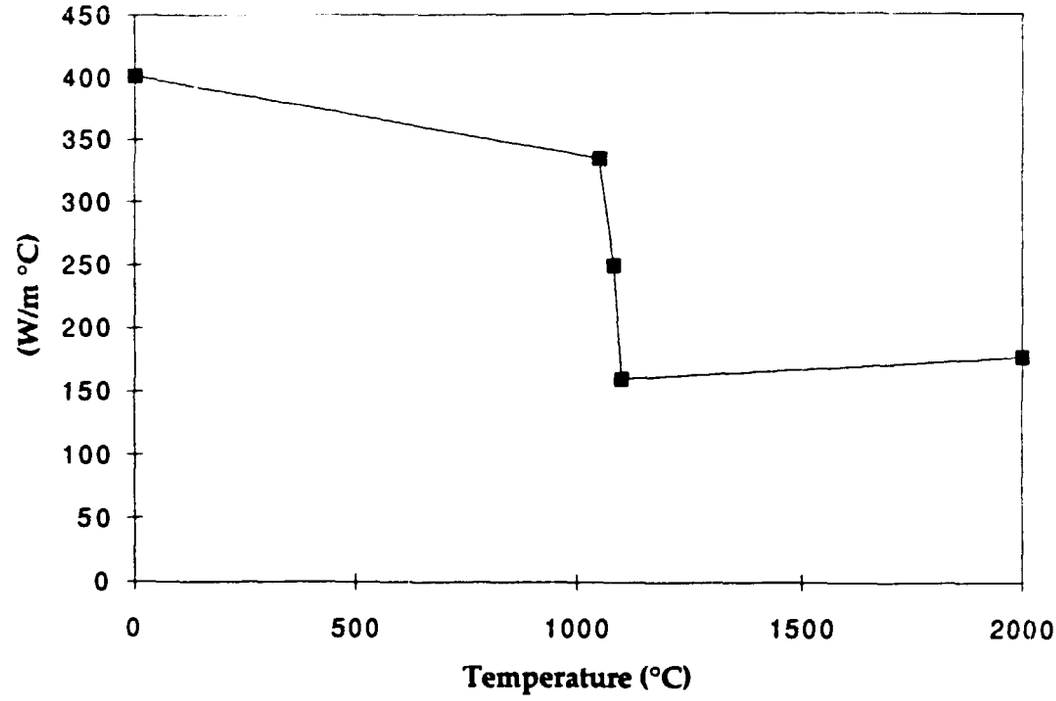

Fig 3a Thermal conductivity as function of temperature for the copper material.

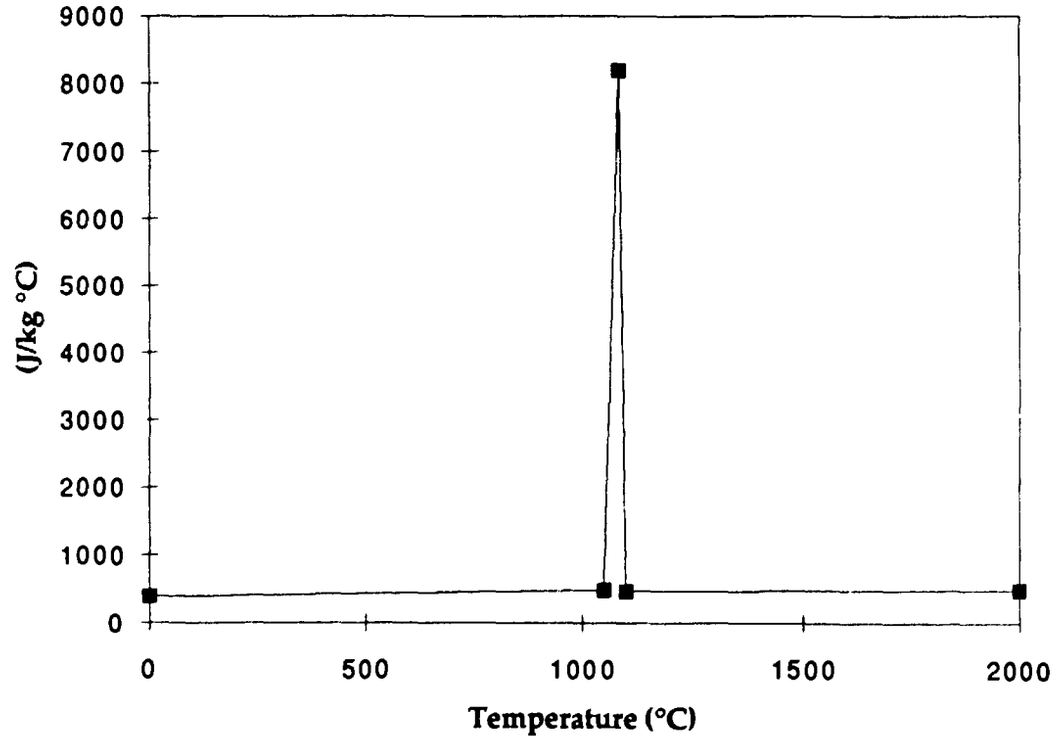

Fig 3b Heat capacity as function of temperature for the copper material.

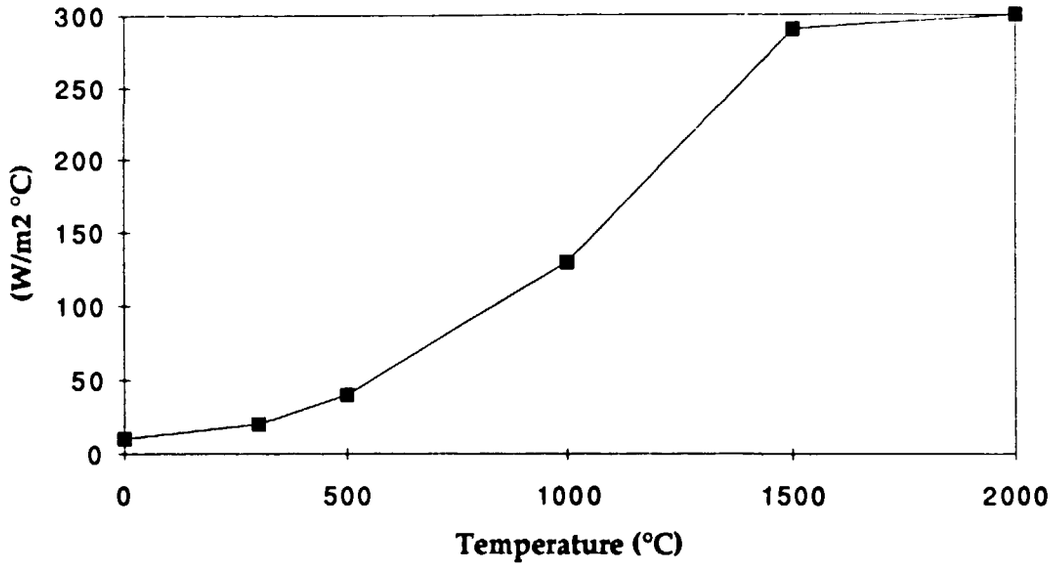

Fig 4 Convective surface heat transfer coefficient as function of temperature.

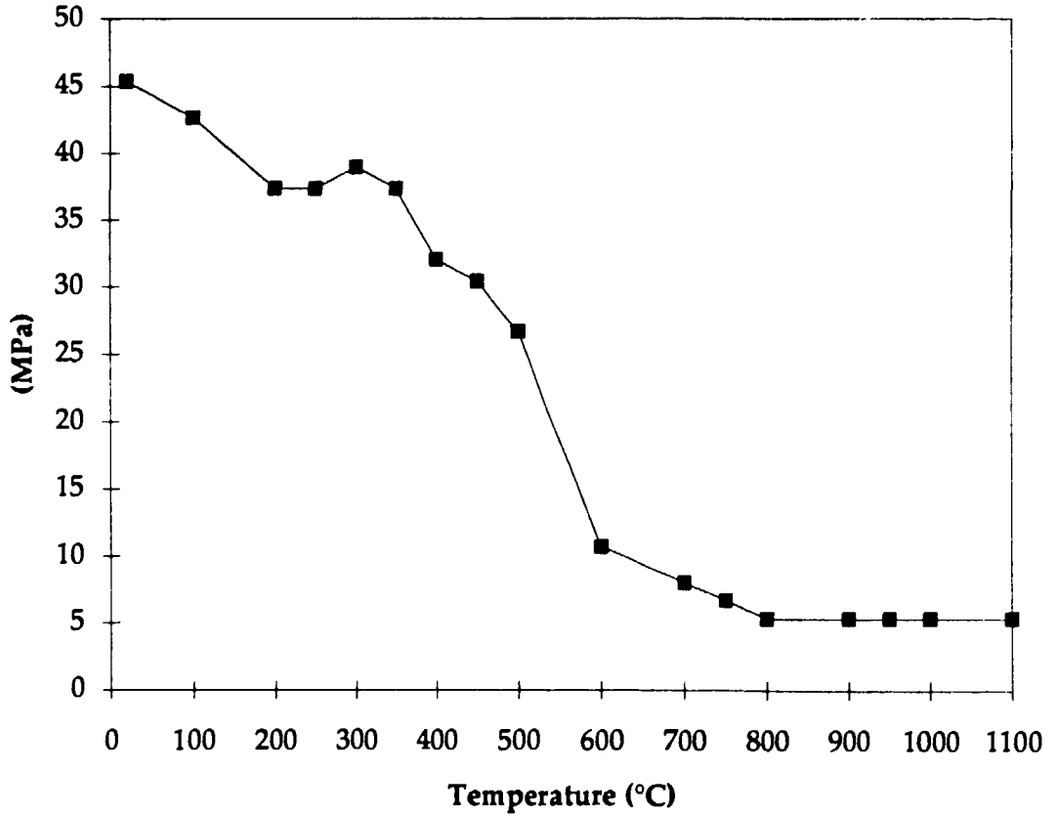

Fig 5 Yield stress as function of temperature for the copper material.

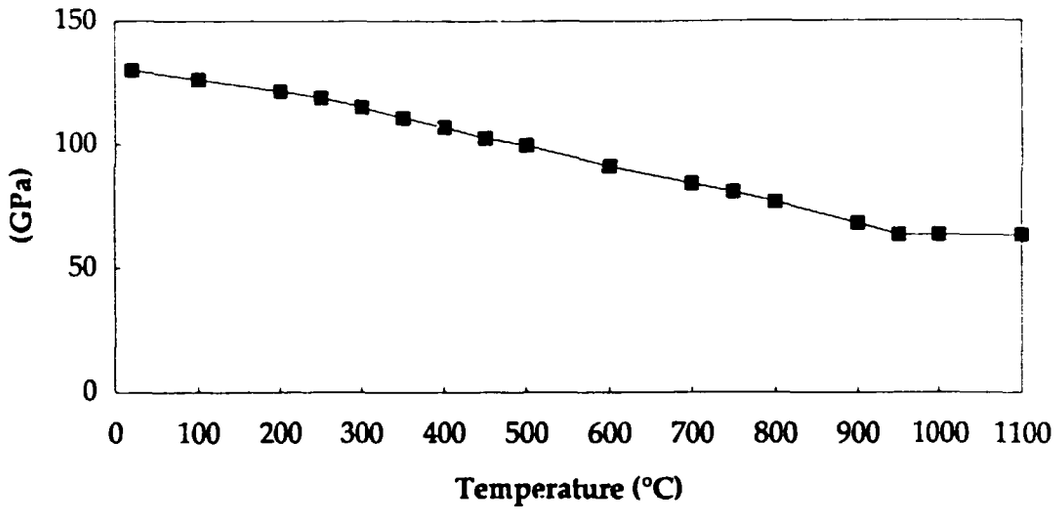

Fig 6 Young's modulus as function of temperature for the copper material.

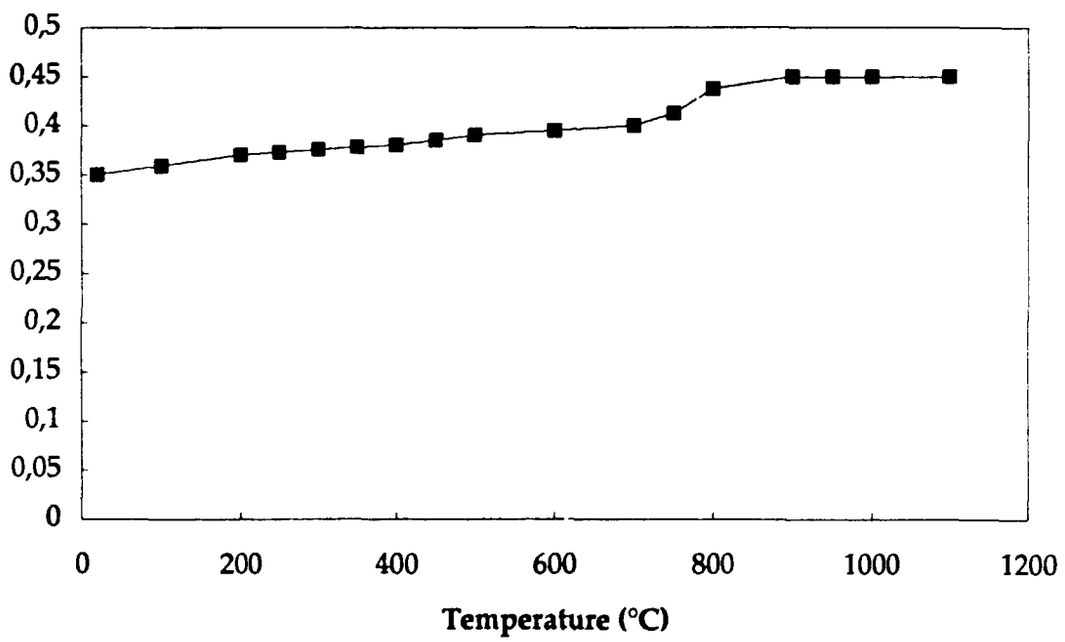

Fig 7 Poisson's ratio as function of temperature for the copper material.

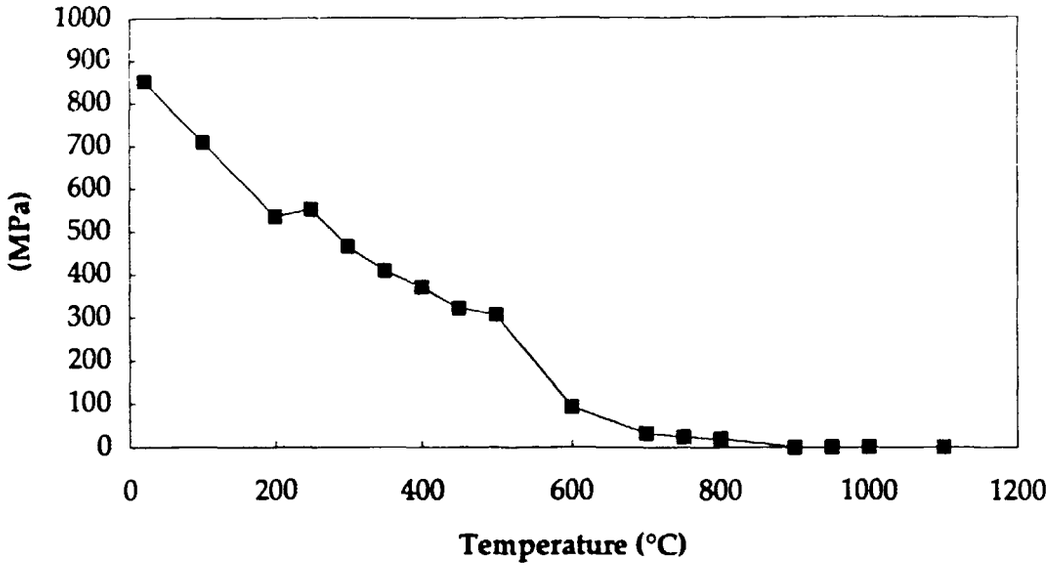

Fig 8 Hardening modulus as function of temperature for the copper material.

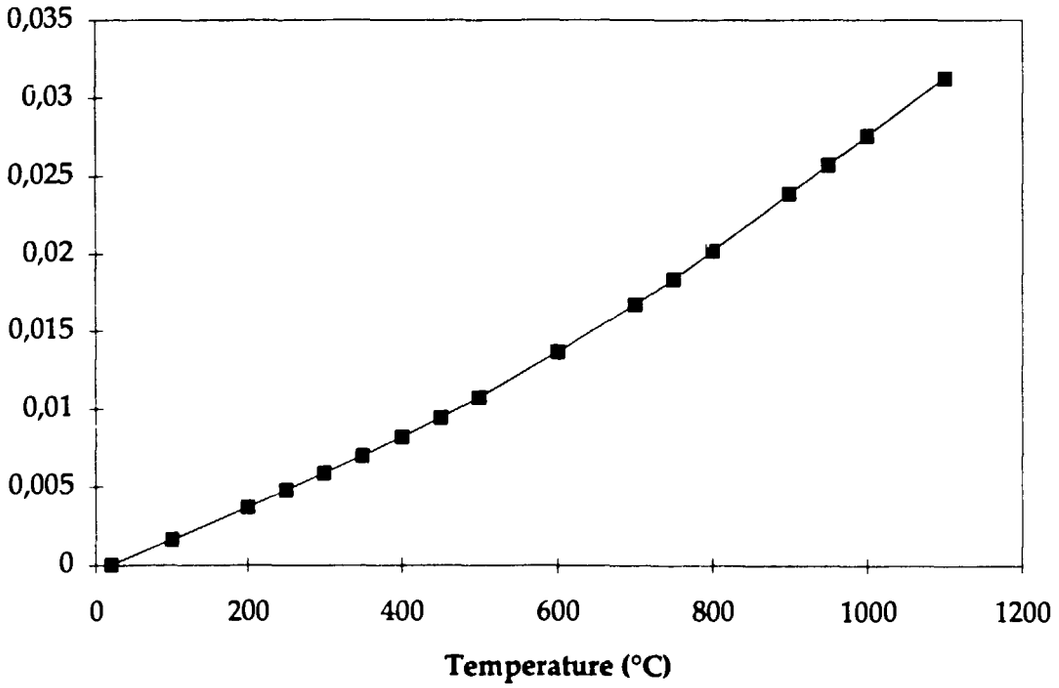

Fig 9 Thermal strain as function of temperature for the copper material.

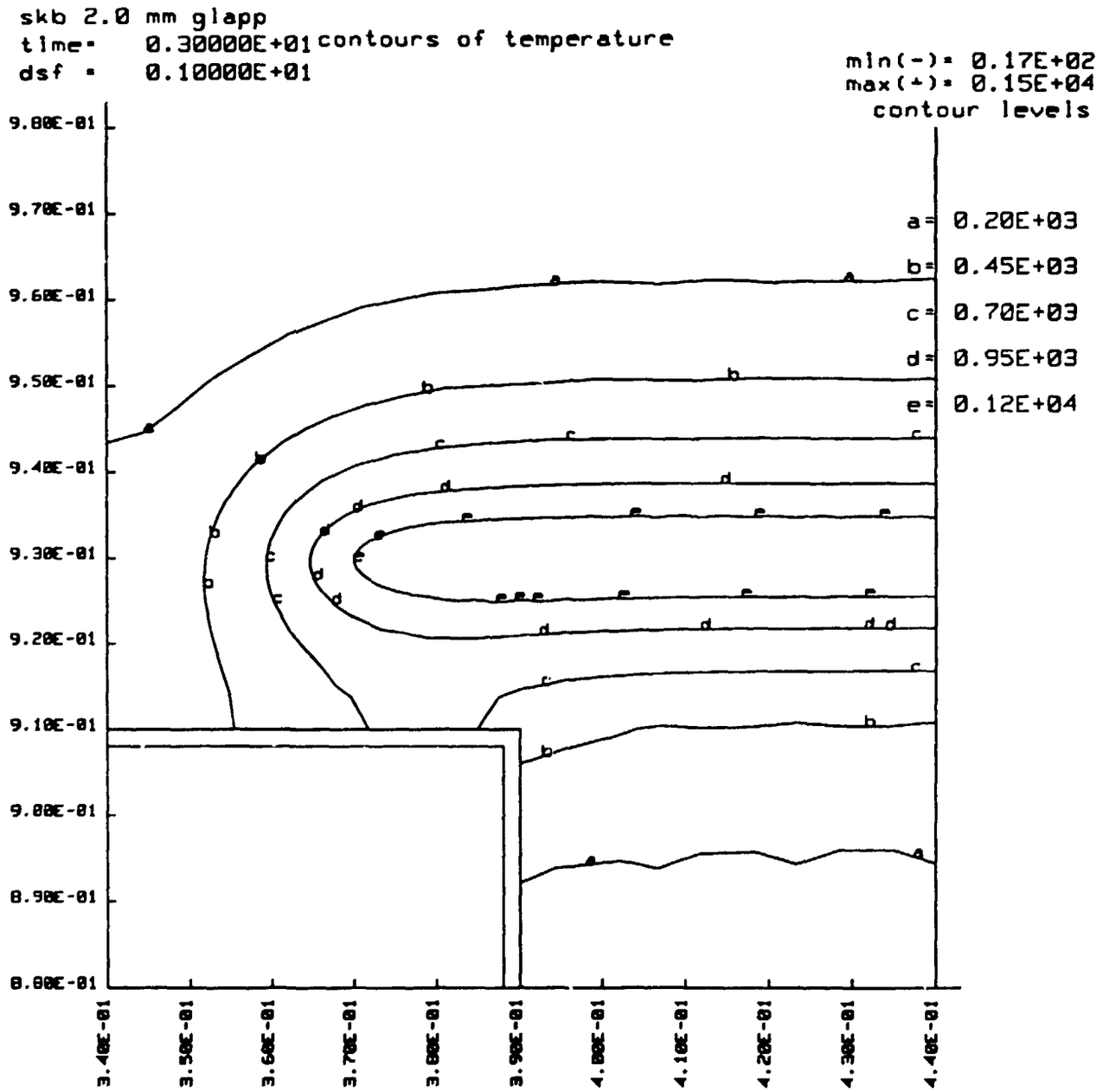

Fig 10 Calculated isotherms during early stage of cooling. Figure is valid for large gap.

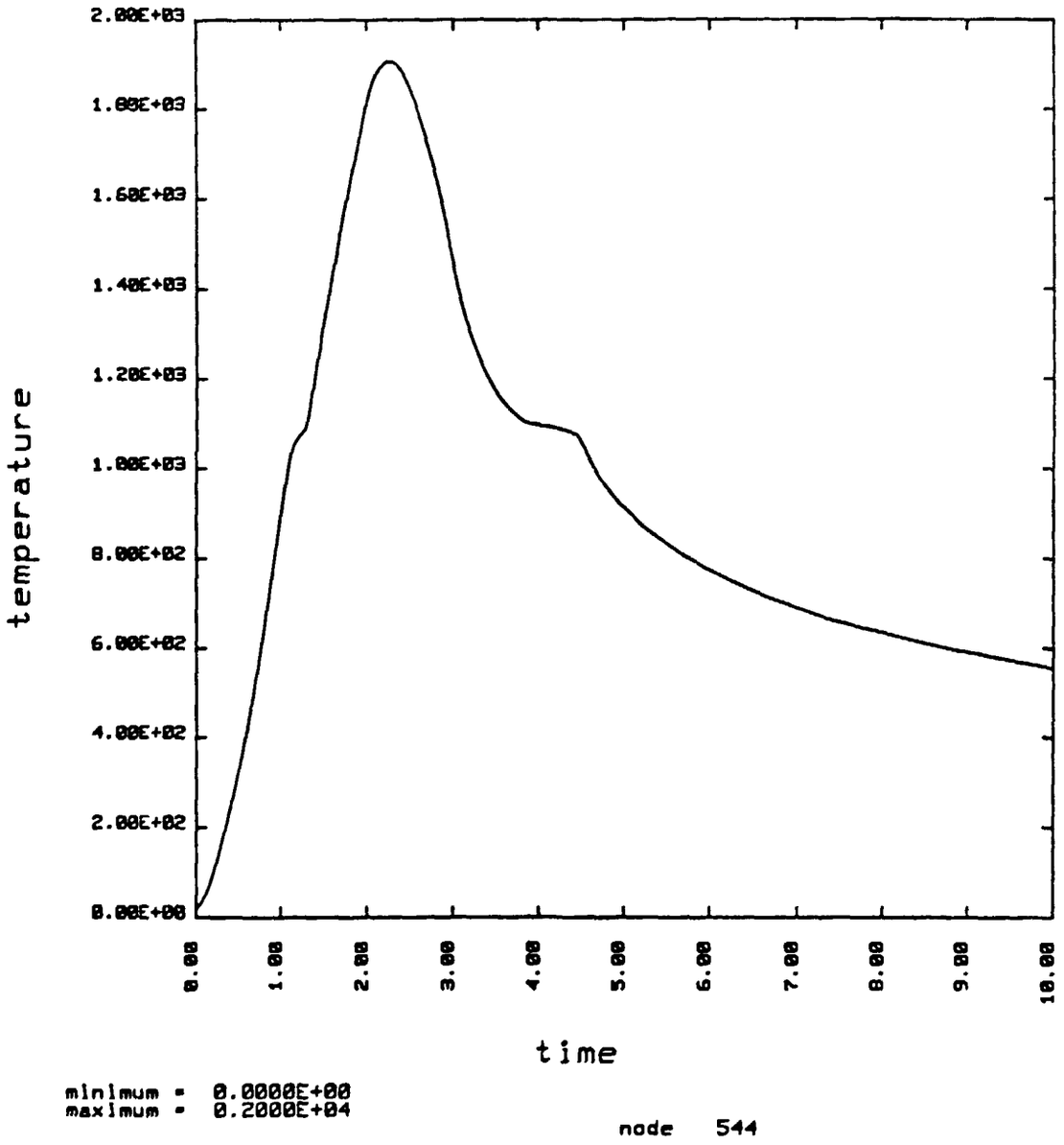

Fig 11 Calculated temperature history for the first 10 seconds at a point within the melted zone.

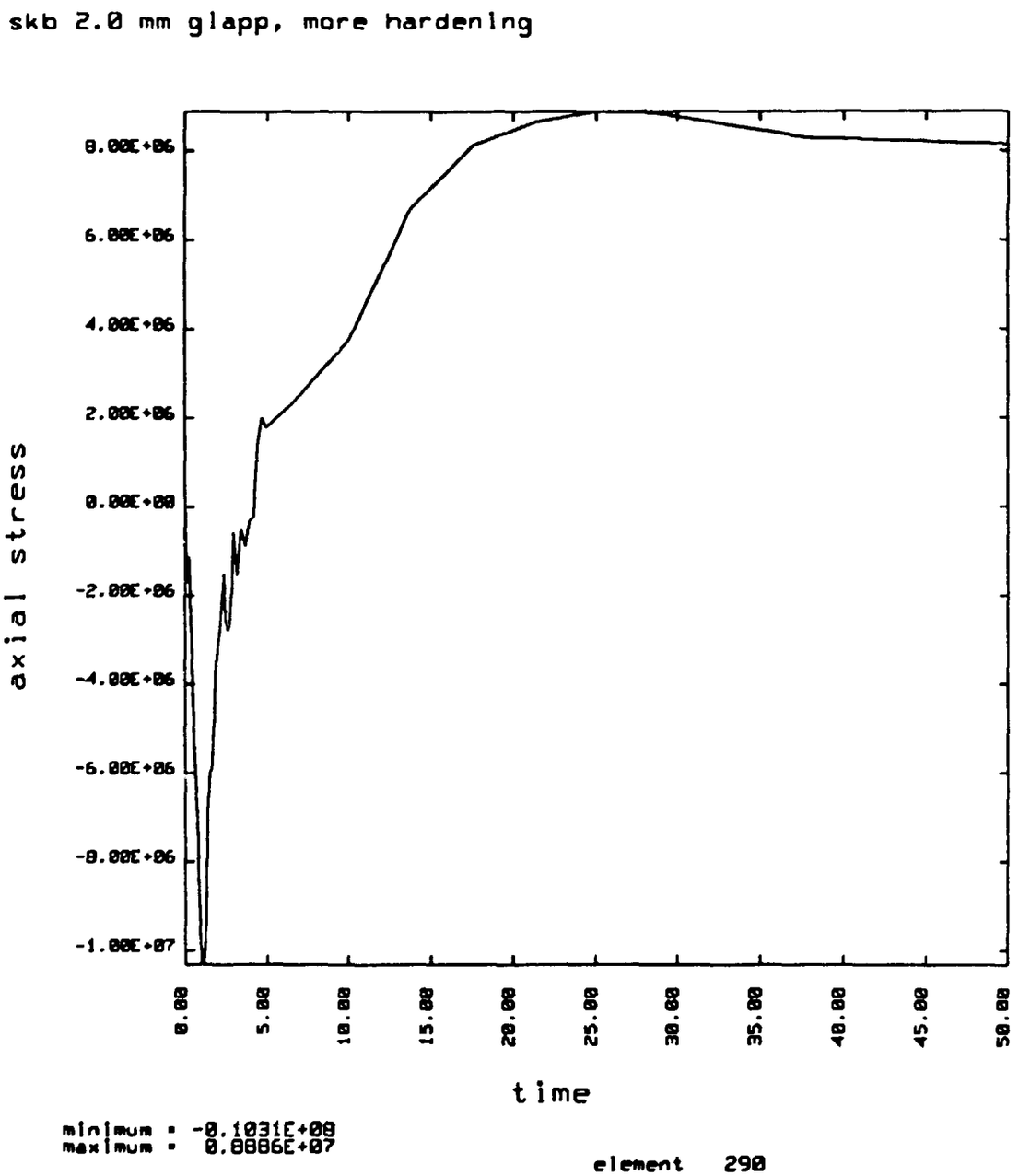

Fig 12a Calculated transient axial stress history for point A of Fig. 2 for large gap 2.0 mm

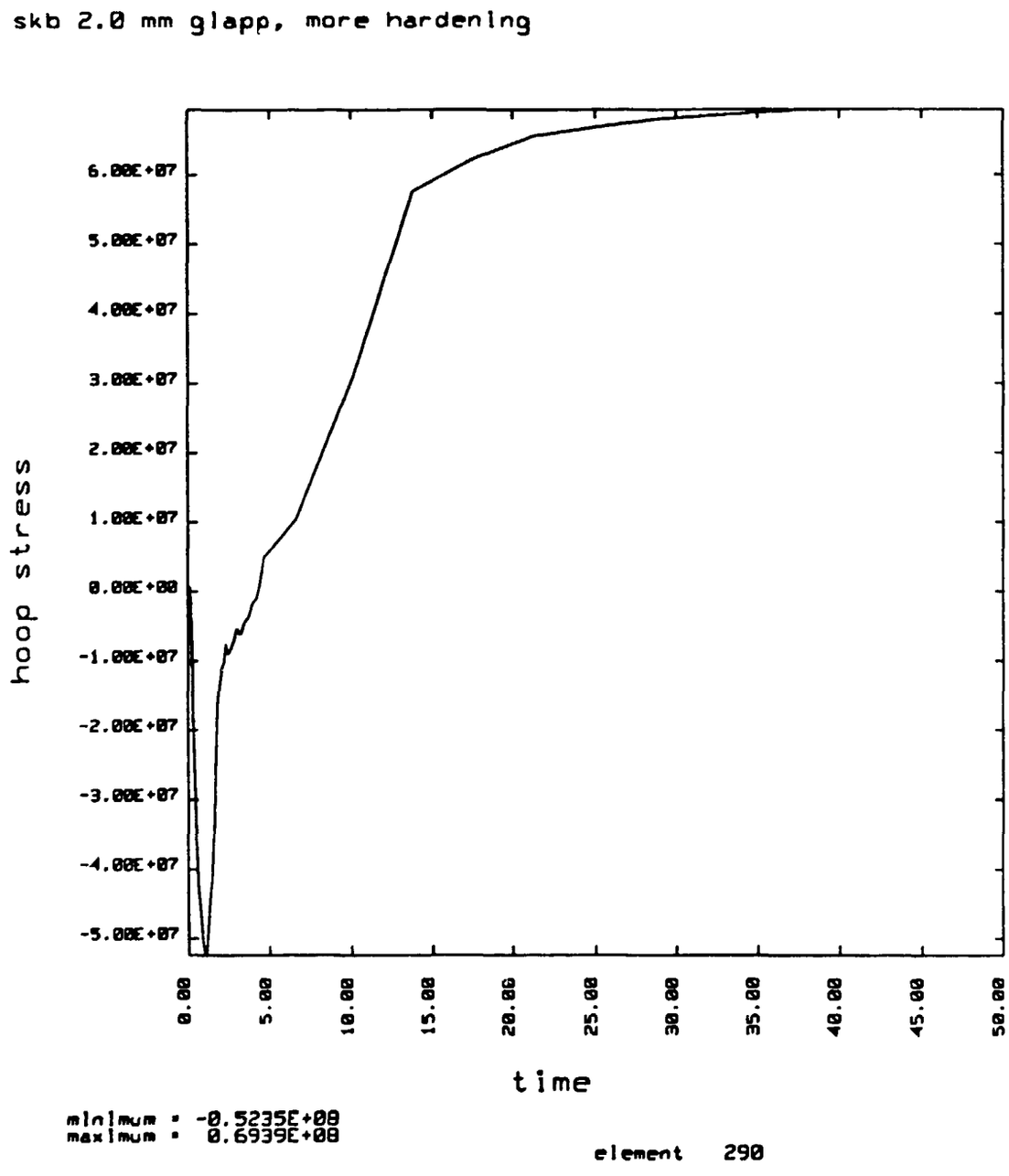

Fig 12b Calculated transient hoop stress history for point A of Fig. 2 for large gap 2.0 mm.

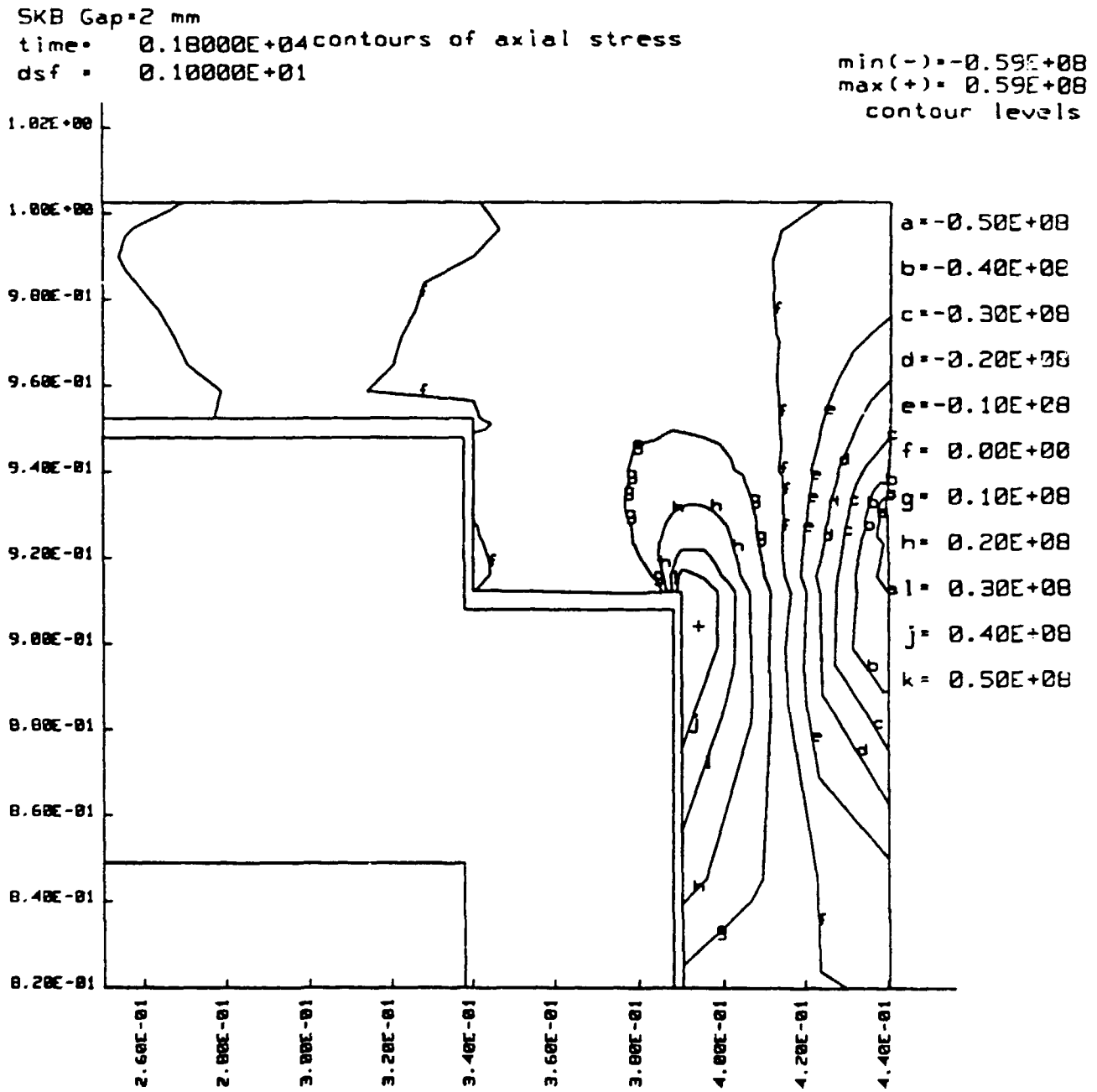

Fig 13a Calculated isolines for welding residual axial stresses for the large gap 2.0 mm.

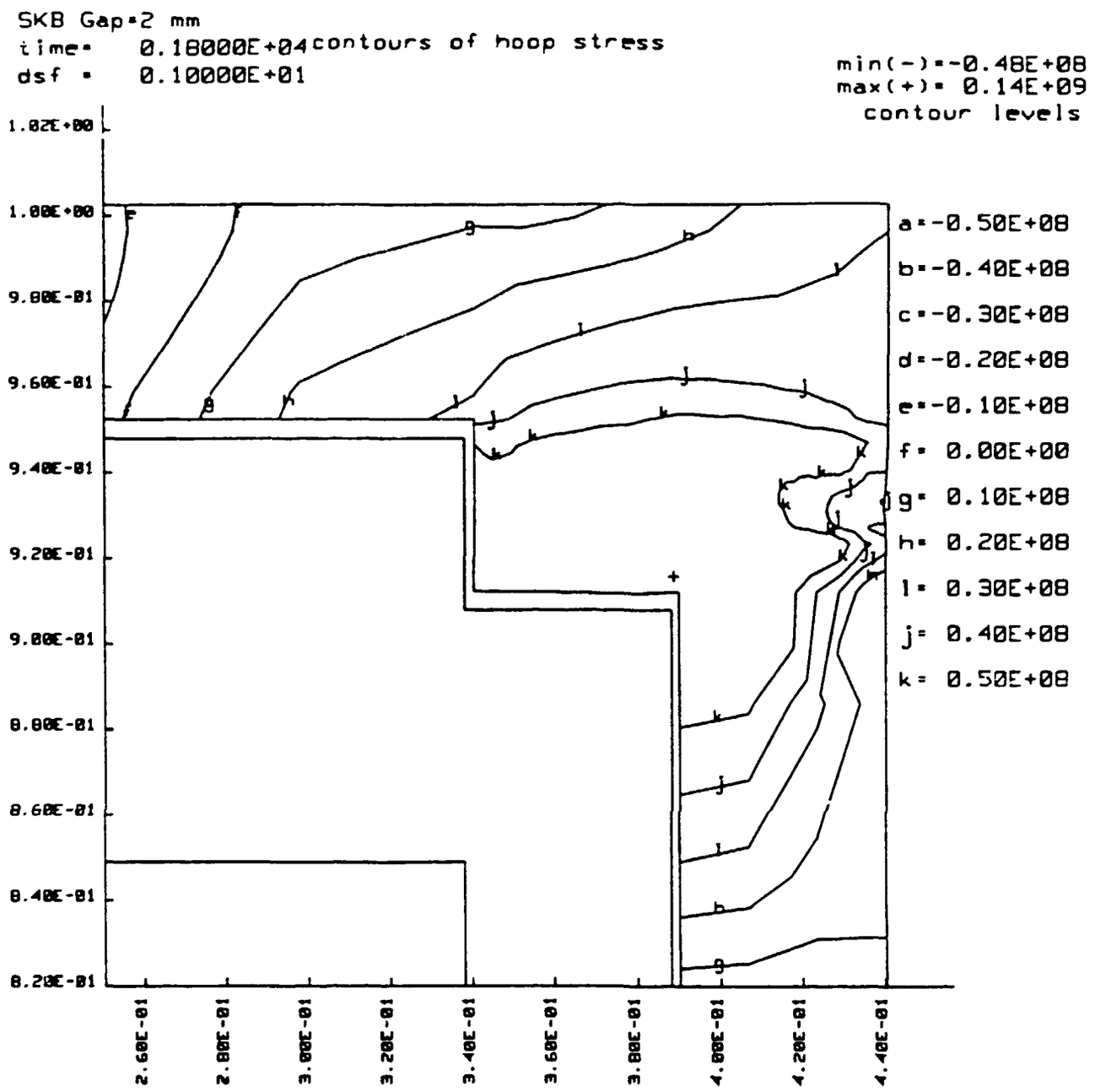

Fig 13b Calculated isolines for welding residual hoop stresses for the large gap 2.0 mm.

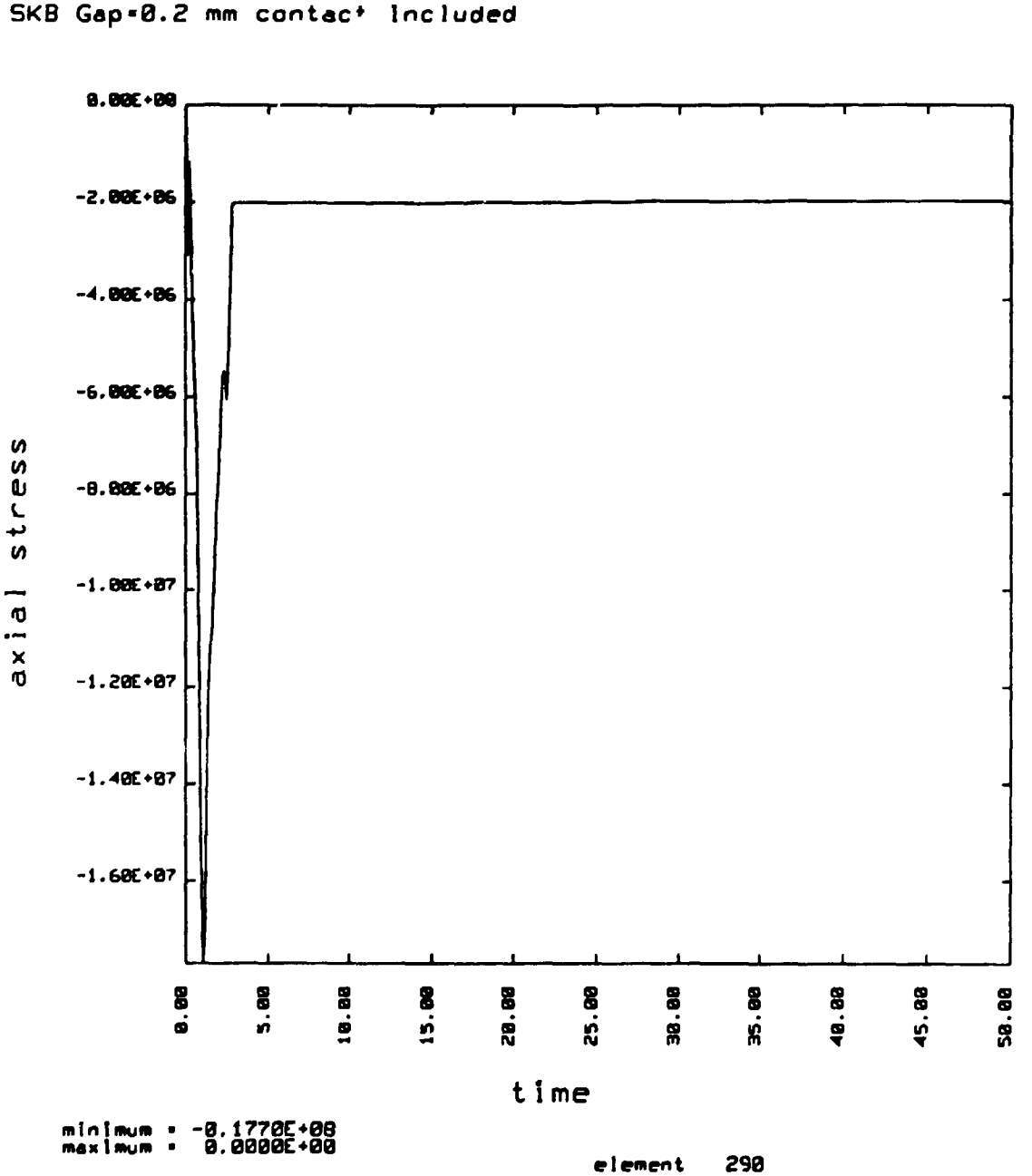

Fig 14a Calculated transient axial stress history for point A of Fig. 2 for small gap 0.2 mm

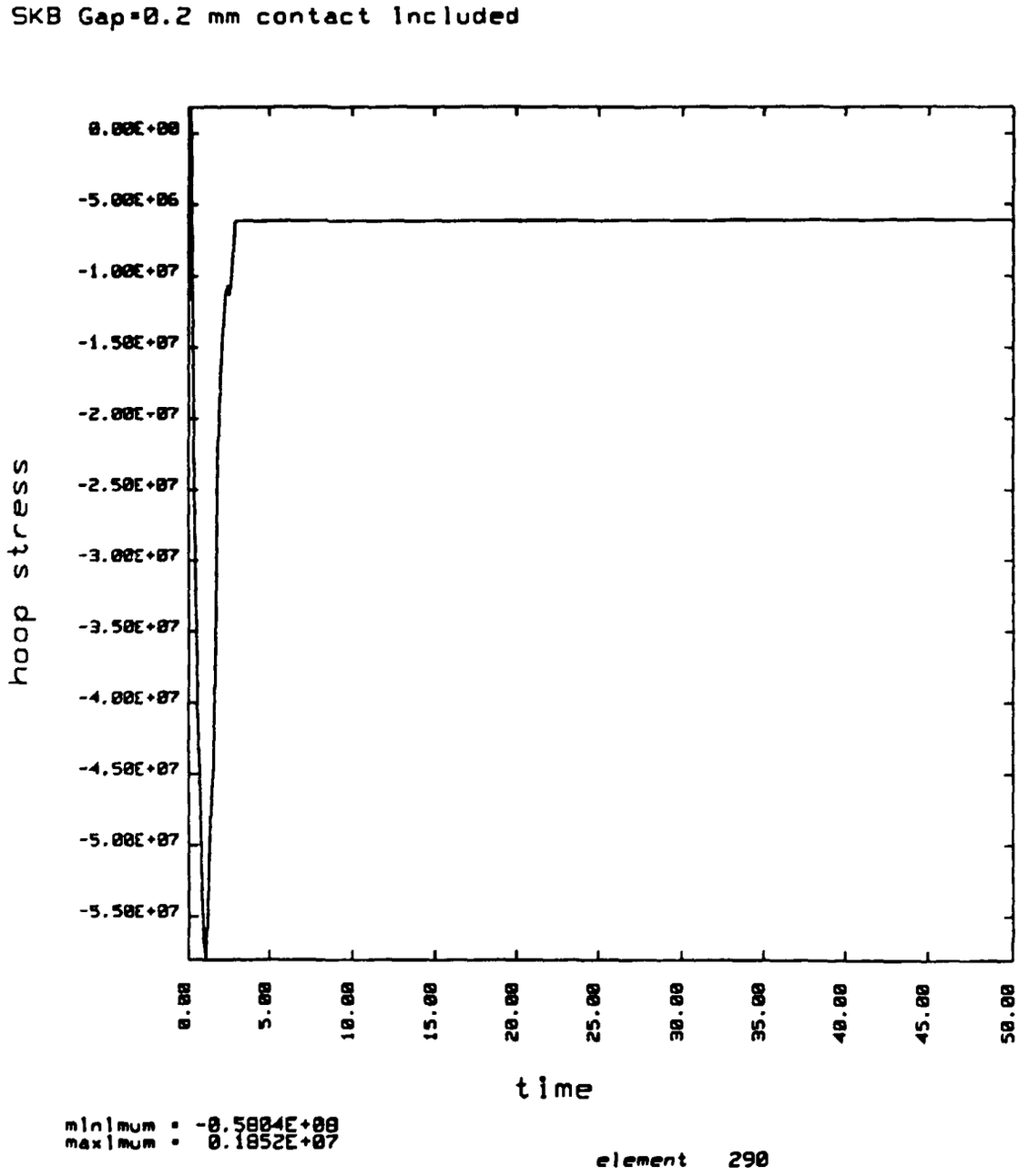

Fig 14b Calculated transient hoop stress history for point A of Fig. 2 for small gap 0.2 mm.

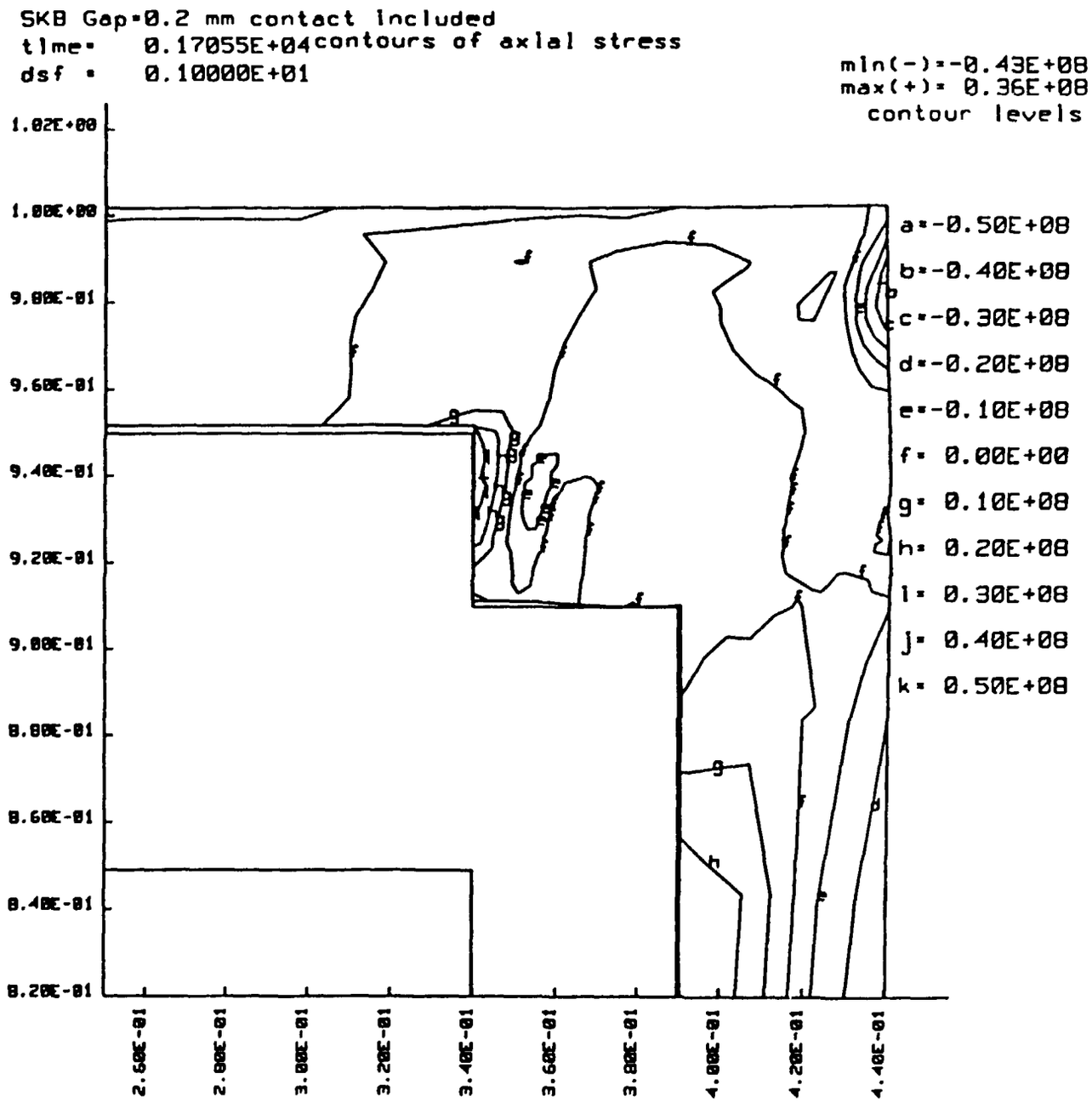

Fig 15a Calculated isolines for welding residual axial stresses for the small gap 0.2 mm.

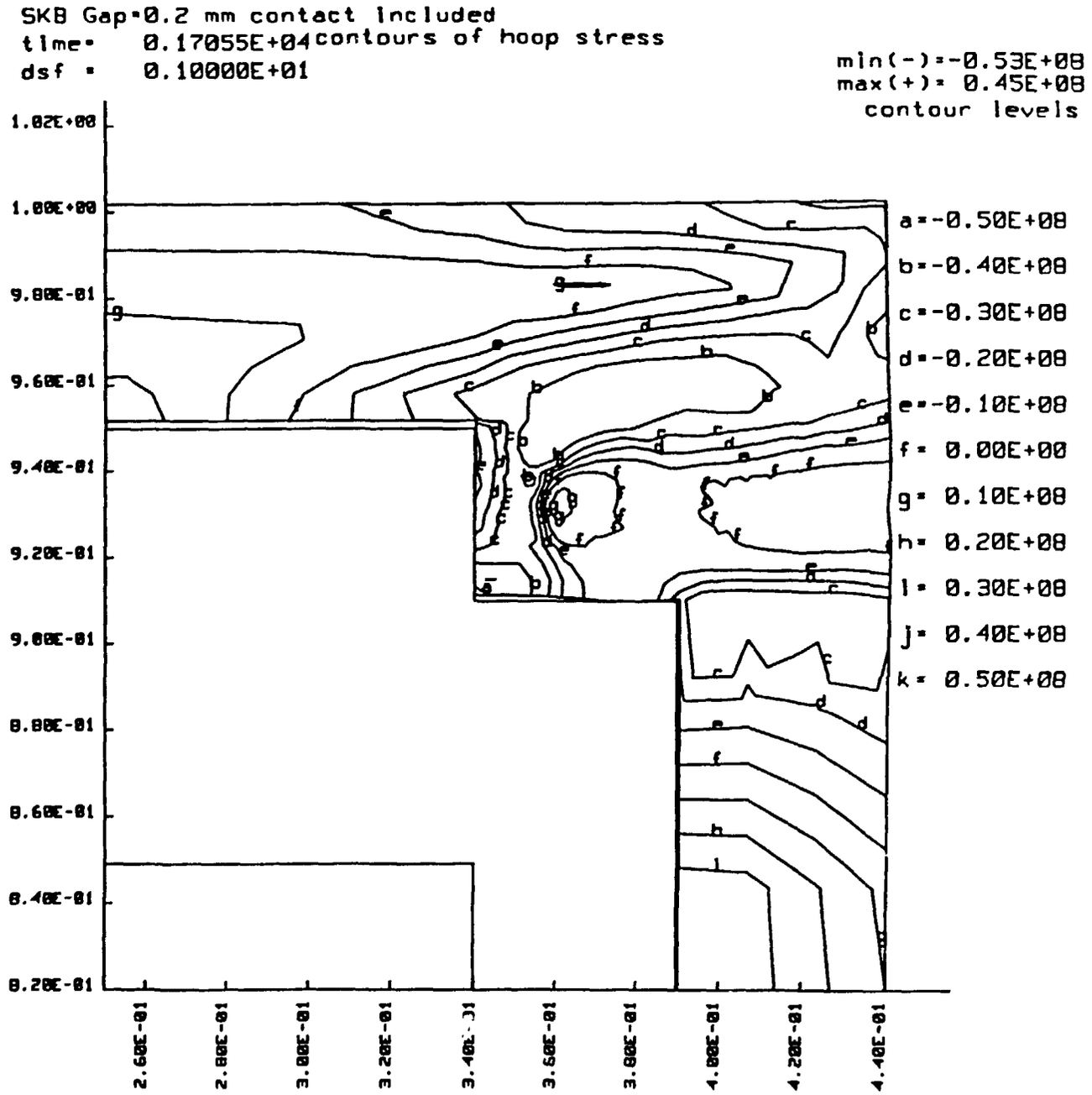

Fig 15b Calculated isolines for welding residual hoop stresses for the small gap 0.2 mm.

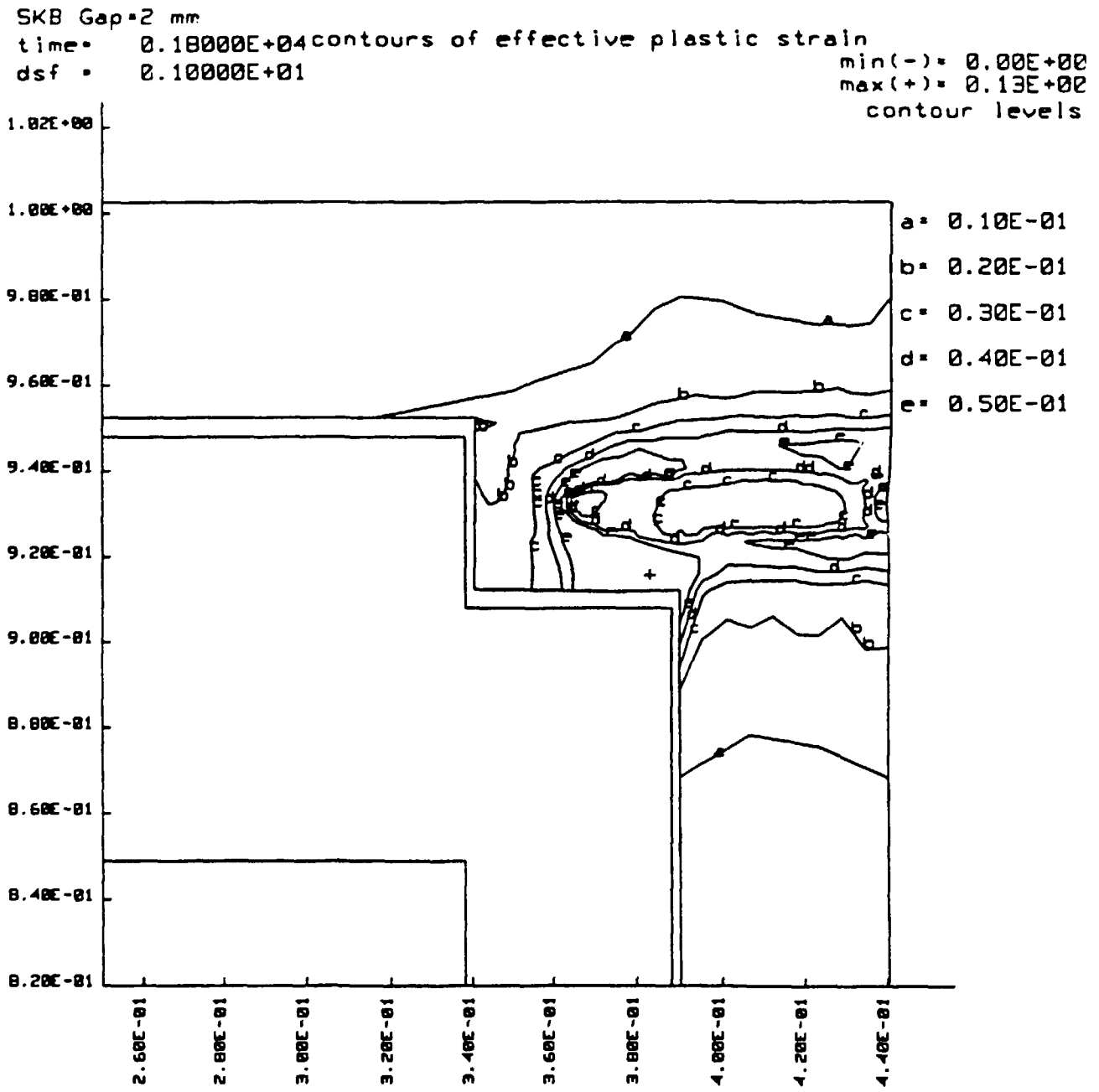

Fig 16 Calculated isolines for accumulated effective plastic strain for large gap 2.0 mm.

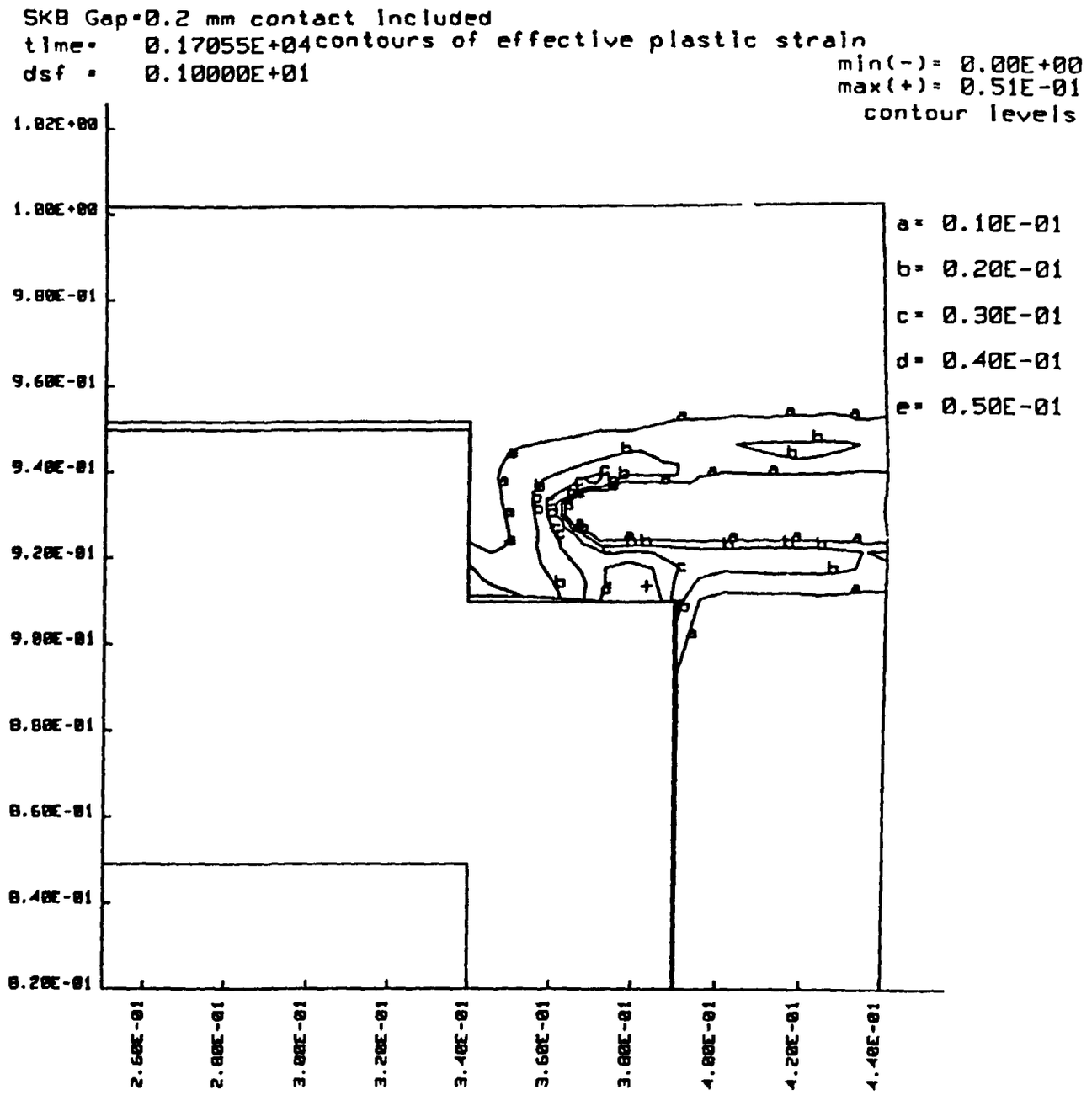

Fig 17 Calculated isolines for accumulated effective plastic strain for small gap 0.2 mm.

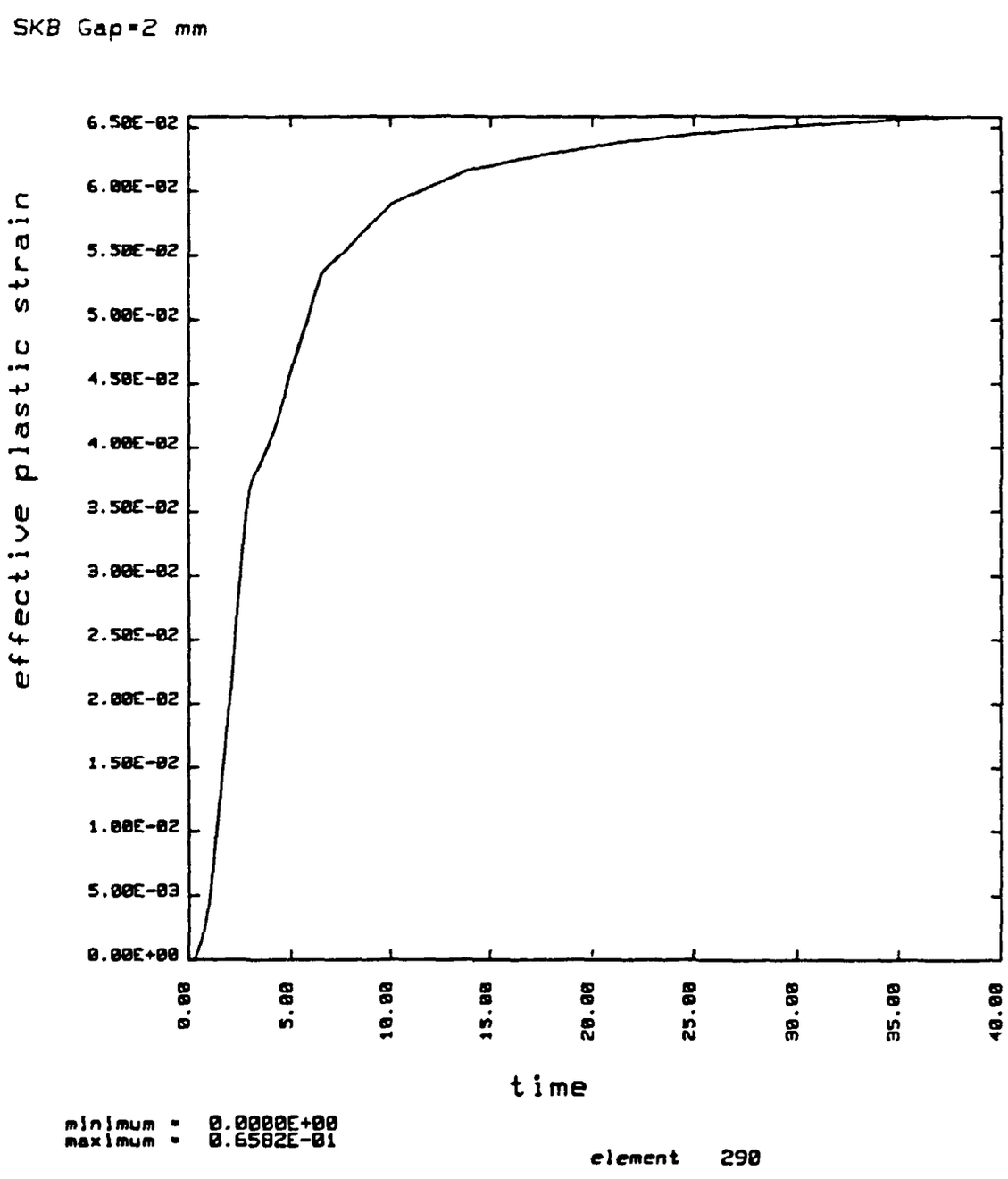

Fig 18 Calculated time history of effective plastic strain for large gap 2.0 mm at a point in the backing ring close to inner surface (r = 0.38 m, z = 0.92 m).

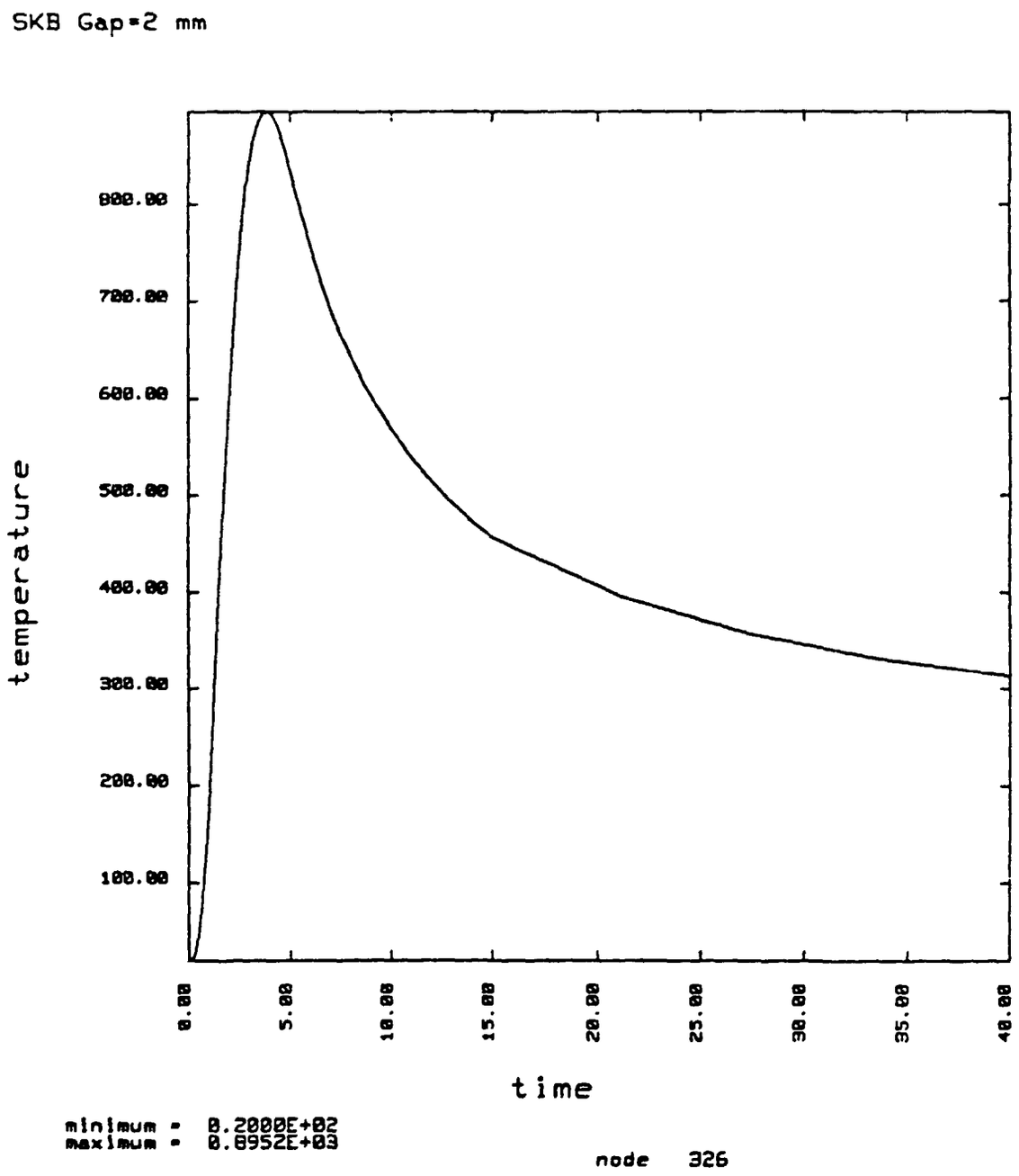

Fig 19 Calculated time history of temperature at a point in the backing ring close to inner surface (same point as in Fig 18).

List of SKB reports

Annual Reports

1977-78
TR 121
KBS Technical Reports 1 – 120
Summaries
Stockholm, May 1979

1979
TR 79-28
The KBS Annual Report 1979
KBS Technical Reports 79-01 – 79-27
Summaries
Stockholm, March 1980

1980
TR 80-26
The KBS Annual Report 1980
KBS Technical Reports 80-01 – 80-25
Summaries
Stockholm, March 1981

1981
TR 81-17
The KBS Annual Report 1981
KBS Technical Reports 81-01 – 81-16
Summaries
Stockholm, April 1982

1982
TR 82-28
The KBS Annual Report 1982
KBS Technical Reports 82-01 – 82-27
Summaries
Stockholm, July 1983

1983
TR 83-77
The KBS Annual Report 1983
KBS Technical Reports 83-01 – 83-76
Summaries
Stockholm, June 1984

1984
TR 85-01
Annual Research and Development Report 1984
Including Summaries of Technical Reports Issued during 1984. (Technical Reports 84-01 – 84-19)
Stockholm, June 1985

1985
TR 85-20
Annual Research and Development Report 1985
Including Summaries of Technical Reports Issued during 1985. (Technical Reports 85-01 – 85-19)
Stockholm, May 1986

1986
TR 86-31
SKB Annual Report 1986
Including Summaries of Technical Reports Issued during 1986
Stockholm, May 1987

1987
TR 87-33
SKB Annual Report 1987
Including Summaries of Technical Reports Issued during 1987
Stockholm, May 1988

1988
TR 88-32
SKB Annual Report 1988
Including Summaries of Technical Reports Issued during 1988
Stockholm, May 1989

1989
TR 89-40
SKB Annual Report 1989
Including Summaries of Technical Reports Issued during 1989
Stockholm, May 1990

1990
TR 90-46
SKB Annual Report 1990
Including Summaries of Technical Reports Issued during 1990
Stockholm, May 1991

1991
TR 91-64
SKB Annual Report 1991
Including Summaries of Technical Reports Issued during 1991
Stockholm, April 1992

Technical Reports

List of SKB Technical Reports 1992

TR 92-01
GEOTAB. Overview
Ebbe Eriksson[1], Bertil Johansson[2], Margareta Gerlach[3], Stefan Magnusson[2], Ann-Chatrin Nilsson[4], Stefan Sehlstedt[3], Tomas Stark[1]
[1]SGAB, [2]ERGODATA AB, [3]MRM Konsult AB
[4]KTH
January 1992

TR 92-02
Sternö study site. Scope of activities and main results
Kaj Ahlbom[1], Jan-Erik Andersson[2], Rune Nordqvist[2], Christer Ljunggren[3], Sven Tirén[2], Clifford Voss[4]
[1]Conterra AB, [2]Geosigma AB, [3]Renco AB,
[4]U.S. Geological Survey
January 1992

TR 92-03
Numerical groundwater flow calculations at the Finnsjön study site – extended regional area
Björn Lindbom, Anders Boghammar
Kemakta Consultants Co, Stockholm
March 1992

TR 92-04
Low temperature creep of copper intended for nuclear waste containers
P J Henderson, J-O Österberg, B Ivarsson
Swedish Institute for Metals Research, Stockholm
March 1992

TR 92-05
Boyancy flow in fractured rock with a salt gradient in the groundwater – An initital study
Johan Claesson
Department of Building Physics, Lund University, Sweden
February 1992

TR 92-06
Characterization of nearfield rock – A basis for comparison of repository concepts
Roland Pusch, Harald Hökmark
Clay Technology AB and Lund University of Technology
December 1991

TR 92-07
Discrete fracture modelling of the Finnsjön rock mass: Phase 2
J E Geier, C-L Axelsson, L Hässler,
A Benabderrahmane
Golden Geosystem AB, Uppsala, Sweden
April 1992

TR 92-08
Statistical inference and comparison of stochastic models for the hydraulic conductivity at the Finnsjön site
Sven Norman
Starprog AB
April 1992

TR 92-09
Description of the transport mechanisms and pathways in the far field of a KBS-3 type repository
Mark Elert[1], Ivars Neretnieks[2], Nils Kjellbert[3], Anders Ström[3]
[1]Kemakta Konsult AB
[2]Royal Institute of Technology
[3]Swedish Nuclear Fuel and Waste Management Co
April 1992

TR 92-10
Description of groundwater chemical data in the SKB database GEOTAB prior to 1990
'Sif Laurent', Stefan Magnusson[2],
Ann-Chatrin Nilsson[3]
[1]IVL, Stockholm
[2]Ergodata AB, Göteborg
[3]Dept. of Inorg. Chemistry, KTH, Stockholm
April 1992

TR 92-11
Numerical groundwter flow calculations at the Finnsjön study site – the influence of the regional gradient
Björn Lindbom, Anders Boghammar
Kemakta Consultants Co., Stockholm, Sweden
April 1992

TR 92-12
HYDRASTAR – a code for stochastic simulation of groundwater flow
Sven Norman
Abraxas Konsult
May 1992

TR 92-13
Radionuclide solubilities to be used in SKB 91
Jordi Bruno[1], Patrik Sellin[2]
[1]MBT, Barcelona Spain
[2]SKB, Stockholm, Sweden
June 1992

TR 92-14
Numerical calculations on heterogeneity of groundwater flow
Sven Follin
Department of Land and Water Resources,
Royal Institute of Technology
June 1992

TR 92-15
Kamlunge study site.
Scope of activities and main results
Kaj Ahlbom[1], Jan-Erik Andersson[2], Peter Andersson[2], Thomas Ittner[2], Christer Ljunggren[3], Sven Tirén[2]
[1] Conterra AB
[2] Geosigma AB
[3] Renco AB
May 1992

TR 92-16
Equipment for deployment of canisters with spent nuclear fuel and bentonite buffer in horisontal holes
Vesa Henttonen, Miko Suikki
JP-Engineering Oy, Raisio, Finland
June 1992

TR 92-17
The implication of fractal dimension in hydrogeology and rock mechanics. Version 1.1
W Dershowitz[1], K Redus[1], P Wallmann[1], P LaPointe[1], C-L Axelsson[2]
[1]Golder Associates Inc., Seattle, Washington, USA
[2] Golder Associates Geosystem AB, Uppsala, Sweden
February 1992

TR 92-18
Stochastic continuum simulation of mass arrival using a synthetic data set. The effect of hard and soft conditioning
Kung Chen Shan[1], Wen Xian Huan[1], Vladimir Cvetkovic[1], Anders Winberg[2]
[1] Royal Institute of Technology, Stockholm
[2] Conterra AB, Gothenburg
June 1992

TR 92-19
Partitioning and transmutation. A review of the current state of the art
Mats Skålberg, Jan-Olov Liljenzin
Department of Nuclear Chemistry, Chalmers University of Technology
August 1992

TR 92-20
SKB 91
Final disposal of spent nuclear fuel. Importance of the bedrock for safety.
SKB
May 1992

TR 92-21
The Protogine Zone.
Geology and mobility during the last 1.5 Ga
Per-Gunnar Andréasson, Agnes Rodhe
September 1992

TR 92-22
Klipperås study site.
Scope of activities and main results
Kaj Ahlbom[1], Jan-Erik Andersson[2], Peter Andersson[2], Tomas Ittner[2], Christer Ljunggren[3], Sven Tirén[2]
[1]Conterra AB
[2]Geosigma AB
[3]Renco AB
September 1992

TR 92-23
Bedrock stability in Southeastern Sweden. Evidence from fracturing in the Ordovician limestones of Northern Öland
Alan Geoffrey Milnes[1], David G Gee[2]
[1]Geological and Environmental Assessments (GEA), Zürich, Switzerland
[2]Geologiska Institutionen, Lund, Sweden
September 1992

TR 92-24
Plan 92
Costs for management of the radioactive waste from nuclear power production
Swedish Nuclear Fuel and Waste Management Co
June 1992

TR 92-25
Gabbro as a host rock for a nuclear waste repository
Kaj Ahlbom[1], Bengt Leijon[1], Magnus Liedholm[2], John Smellie[1]
[1]Conterra AB
[2]VBB VIAK
September 1992

TR 92-26
Copper canisters for nuclear high level waste disposal. Corrosion aspects
Lars Werme, Patrik Sellin, Nils Kjellbert
Swedish Nuclear Fuel and Waste Management Co, Stockholm, Sweden
Oktober 1992